Stress-strain behavior and liquefaction strength characteristics of Ottawa F65 sand

Mohamed A. ElGhoraiby^{1*}, Hanna Park¹ and Majid T. Manzari ¹

Abstract

The stress-strain-strength response of soils is of significant interest to development and calibration of realistic constitutive models that can be used in numerical simulation of geotechnical engineering problems. An extensive characterization of Ottawa F65 sand along with various monotonic and cyclic tests conducted during the course Liquefaction Experiments and Analysis Projects (LEAP) are presented here. The specimens in these tests were prepared using a meticulous sample preparation technique which guaranteed consistency and repeatability. Monotonic drained and undrained triaxial tests shed light on the steady-state (critical state) of Ottawa sand, while stress-controlled and strain-controlled cyclic triaxial and direct simple shear tests provide key information on the cyclic stress-strain behavior and liquefaction strength of this soil. The triaxial tests identify the liquefaction strength of the soil at different densities, while the direct simple shear tests evaluate the effect of overburden pressure on the cyclic response. The results of these experiments are also compared to the experimental results available in the literature. The data obtained from the cyclic triaxial and direct simple shear tests were further analyzed by plotting the computed shear modulus degradation and damping curves. The results show how the soil stiffness degrades as cyclic shear stress is applied for soil at different densities and confining stresses. It can be seen that the rate of shear modulus degradation increases with the increase of confining stress and decreases with the increase of soil density. The damping curves consistently show an increasing in damping ratio until a shear strain of about 0.05%, followed by a plateau at about 20-25% damping ratio for shear strain between 0.05 and 0.5%, and ending with a decrease in damping until reaching a final damping ratio of about 10%.

¹ Department of Civil and Environmental Engineering, George Washington University, Washington, DC, USA.

^{*} Corresponding Author, ghoraiby@gwu.edu.

1. Introduction

In this paper, the cyclic stress-strain response of Ottawa F65 sand is evaluated and the liquefaction strength is assessed through extensive laboratory experiments. The experiments include a series of stress-controlled cyclic triaxial tests conducted on Ottawa F65 sand. In addition, strain-controlled cyclic triaxial tests were performed. The tests were conducted on samples prepared at three different densities. Finally, the presented work includes cyclic direct simple shear tests intended to investigate the effects of overburden stresses on the cyclic response of the soil.

Laboratory element tests such as triaxial and direct simple shear have been used to understand and characterize the cyclic response of sands. Since the pioneering work of Seed and Lee [1] and Castro [2], a large body of literature has emerged based on the study of liquefaction of sandy soils using element tests. These tests have provided a deeper understanding of the cyclic stress-strain behavior of sand, quantitatively determined the triggering of soil liquefaction, and provided insights on cyclic mobility phenomenon. Moreover, the effects of different factors such as soil fabric, anisotropic consolidation, sample preloading, and presence of fines content, among others, have been investigated and reported extensively in the literature.

Soil liquefaction is defined as the state at which the soil loses its shear stiffness [3]. When the soil is sheared, it experiences a change in volume. This change translates to excess pore water pressure generation in an undrained condition, where a contractive response results in a positive excess pore pressure and a dilative response results in a negative excess pore pressure. Under cyclic shearing, excess pore water pressure will generate which leads to a reduction in the effective stress and in turn the soil stiffness.

As the effective stress and soil stiffness reach zero, large shear strains begin to develop. At this point, the soil is considered to have reached the state of liquefaction. The term "initial liquefaction" was defined by Seed as the first time the soil reaches the zero effective stress [1]. Beyond this point the soil response cycles between dilating and regaining some of its shear stiffness, and contracting and losing the stiffness upon load reversal. This response is depicted by the commonly observed butterfly response of the effective stress path.

A distinction is made between the sudden failure of the soil known as the flow liquefaction and the progressive failure due to soil softening known as the cyclic mobility [4]. Flow liquefaction is observed in loose contractive soils where the effective stress suddenly reaches zero and large shear strain develops. The cyclic mobility of soil is that gradual increase in the shear strains developed over cycles as the soil stiffness gradually degrades. This response is observed in denser or more dilative soil.

The liquefaction strength has been quantified as the number of shear stress or strain cycles it takes until soil liquefaction is reached. The criteria for soil liquefaction is dependent on the mode of failure (flow liquefaction or cyclic mobility) and the type of test conducted (stress-controlled or strain-controlled). In the case of a strain-controlled test or when flow liquefaction is expected, it

is natural to define the criteria for liquefaction to be the point at which the soil reaches zero effective stress. However, in the case of a stress-controlled test on dense soil where cyclic mobility is expected a liquefaction criterion based on the magnitude of shear strain is more suitable. Different shear strain amplitudes have been set as the liquefaction criteria for soil ranging from 2% single amplitude of shear strain up to 10 % double amplitude [5].

The liquefaction strength of the soil is affected by different factors. Besides the soil density and shear stress magnitude, factors such as the initial confining stress and initial shear as well as the soil fabric can affect the liquefaction resistance of the soil. As the magnitude of confining stress increases, the number of cycles required to reach liquefaction decreases for a given cyclic stress ratio [6]. Based on this observation, a correction factor K_{σ} has been proposed to account for the reduction in the resistance due to the increase in the confining stress with respect to the strength of the soil at 100 kPa.

In cases where the ground is sloping, static shear stress has to be considered. The static shear stress can affect the cyclic resistance of the soil. Another correction factor, K_{α} , where α is the ratio of the static shear stress over the mean effective stress. The K_{α} factor is defined as the ratio of the cyclic resistance ratio (CRR) obtained for specific static shear stress over the CRR where no static shear stress is applied [5]. Vaid and Finn [7] have shown that dependence of the K_{α} on the assumed failure criterion. They showed that if a shear strain amplitude considered for failure is 2%, a decrease in the CRR is observed as the α increases. On the other hand, if a shear strain amplitude of 5% is assumed, an increase in CRR is shown with the increase of α . Rollins and Seed [8] have shown that dependency of K_{α} on the soil's relative density, D_{r} . It was shown that soil with a D_{r} of 35% yields a decreasing K_{α} as α increases, while an increase is observed for a soil with a D_{r} of 55%.

The cyclic resistance of sand has also been observed to be highly affected by soil fabric and sample preparation methods. Mulilis et al. [9] have shown that the cyclic resistance of the samples prepared with different placement and different compaction may be very different. In the work of Mulilis et al. (1975), the specimens were prepared by moist or dry deposition, while the compaction was done with high-frequency vibration, tamping, rodding as well as dry and wet pluviation. With the significant difference in the liquefaction strength curves, it is clear that it is important for the sample preparation for laboratory tests to more closely mimic the field condition. The results showed that the dry pluviation resulted in the lowest cyclic resistance while the moist placement resulted in higher cyclic resistance than the dry placement.

Since the experiments reported in this paper were conducted as part of the Liquefaction Experiments and Analysis Projects [10–12], the sample preparation technique was the constant height dry pluviation method which was also used in the LEAP-GWU-2015 [13], LEAP-UCD-2017 [14] and LEAP-Asia-2019 centrifuge experiments [15].

Previous experimental studies conducted on Ottawa F65 sand included cyclic triaxial (Vasko, 2015) as well as cyclic direct simple shear tests (Bastidas 2016). Vasko [16,18] conducted a series of triaxial experiments for the planning phase of the liquefaction experiments and analysis project (PLEAP, aka LEAP-GWU-2015). The experimental data reported by Vasko (2015) were used in a numerical prediction exercise where five centrifuge tests modeling lateral spreading of liquefiable sloping ground were predicted by several numerical simulation teams [10]. The cyclic triaxial tests by Vasko (2015) were performed for a single soil density to match the centrifuge tests target density. The specimens were prepared by using dry pluviation with minor tapping on the mold. Bastidas (2016) also produced an extensive dataset of monotonic and cyclic direct simple shear experiments on Ottawa F65 sand for two different densities. Dry funnel deposition was the sample preparation method for the loose specimen, while air pluviation was used for dense soil. In addition to these experiments cyclic torsional shear tests were conducted at the University of Kyoto as part of the LEAP-Asia-2019 project [19].

In the following sections, the results of a large number of cyclic triaxial and direct simple shear tests on Ottawa F65 are presented and analyzed. First, a brief description of Ottawa F65 composition, characteristics and soil properties is presented. Shear strength of the soil under monotonic triaxial compression are briefly presented next. The results of a series of cyclic stress-controlled and cyclic strain-controlled tests are then summarized. Afterwards, the observed response of Ottawa sand in cyclic direct simple shear tests is presented. The effects of overburden pressure on the liquefaction strength of the soil are discussed next. Finally, additional observations and data analysis are presented and discussed.

2. Ottawa F65 Sand Soil Characteristics

Ottawa F65 sand is a clean poorly graded sand produced by US Silica, in Ottawa, Illinois. This soil is a selected as the soil of choice by a consortium of centrifuge laboratories to study the soil liquefaction as part of the Liquefaction Experiments and Analysis Projects (LEAP). It consists of over 99% silica and less than 1% fines content. The soil particles are sub-rounded as shown in Figure 1. A large number of characterization tests were conducted on five different batches of soil delivered to the George Washington University soil mechanics laboratory. The results showed consistency and uniformity among different batches. Ottawa sand has a specific gravity of 2.65 with coefficient of variation of 0.8%. The average particle size distribution obtained from sieve analysis conducted on samples from each batch is shown in Figure 1.

A series of constant head hydraulic conductivity tests were conducted to determine the permeability of the Ottawa F65 sand at different densities. The tests followed the ASTM D 2434 standard testing procedures. The coefficient of hydraulic conductivity ranged from 0.008 to 0.015 cm/sec for the samples prepared at void ratios ranging from 0.486 to 0.766. The following relationship between the soil void ratio (e₀) and soil hydraulic conductivity (k) was obtained from the test results,

$$k(\text{cm/s}) = 0.0207 \, e_o - 0.0009 \tag{1}$$

Over the past few years, a large number of tests (Vasko 2015; Bastidas 2016; Carey et al. 2017; Kutter et al. 2017) have been performed to obtain maximum and minimum void ratios of Ottawa F65 sand. The results reported by different researchers showed significant scatter. Hence, in order to ensure consistency among the participating research groups, a single set of maximum and minimum void ratios were adopted by LEAP researchers. These values are 0.78 and 0.51 for maximum and minimum void ratios, respectively. Additional details about the soil characterization tests can be found in the following references [21–23].

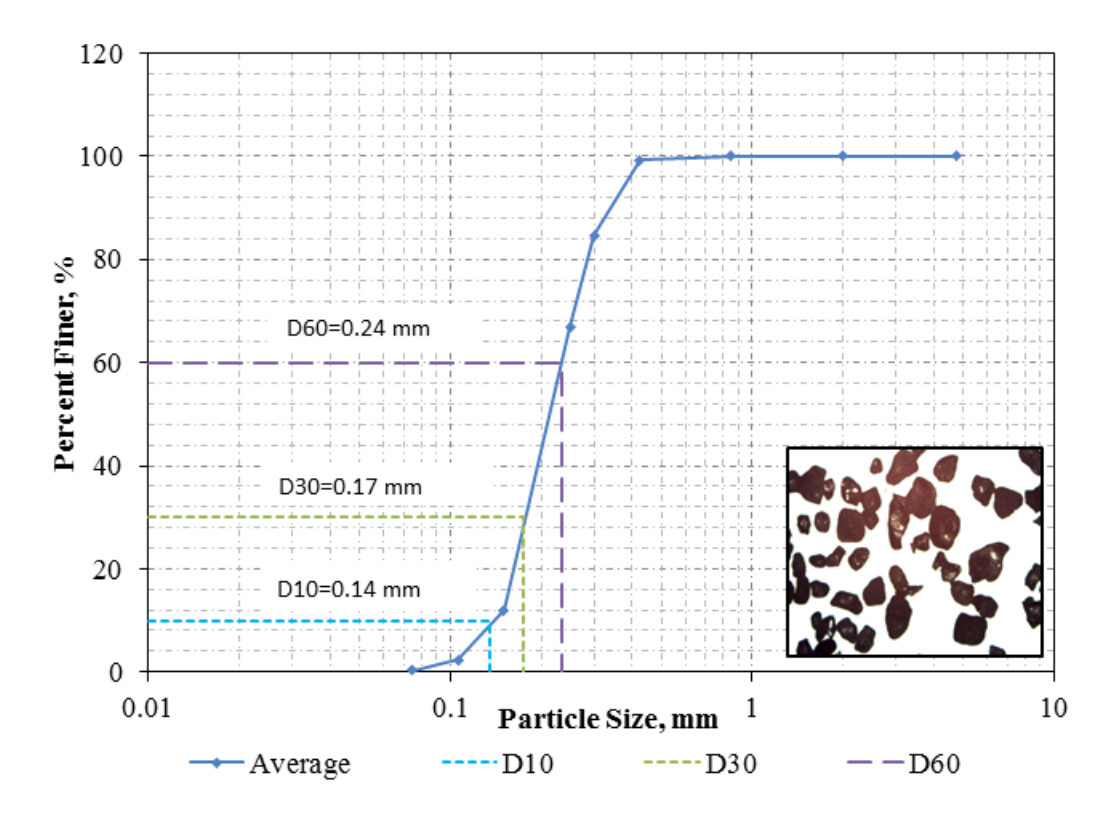


Figure 1: Ottawa F65 Average Particle-Size Distribution

3. Shear strength in monotonic triaxial tests

A number of drained and undrained triaxial compression tests were conducted to investigate the shear strength of Ottawa F65 sand. Figure 2 shows the results obtained from drained tests conducted on the specimens with various initial densities but under similar confining stresses. The plot shows the shear stress and volumetric strain development versus the axial strain for specimens with void ratios ranging from 0.575 up to 0.726 which correspond to relative densities that range from 19% up to 73%. The confining stress applied is between 100 and 120 kPa. Figure 3 shows the stress ratio development against axial strain and void ratio for the same set of tests. It can be seen from all the tests that the soil reaches a critical stress ratio of 1.2 and a friction angle of 30.7°.

Figure 4 shows the critical state envelope obtained from the drained and undrained triaxial experiments performed on Ottawa F65 sand. Details of the monotonic triaxial compression tests will be covered in a separate paper. It is noted, however, that the data on Figure 4 includes a number of undrained triaxial compression tests at higher confining stresses ranging from 500 to 1000 kPa.

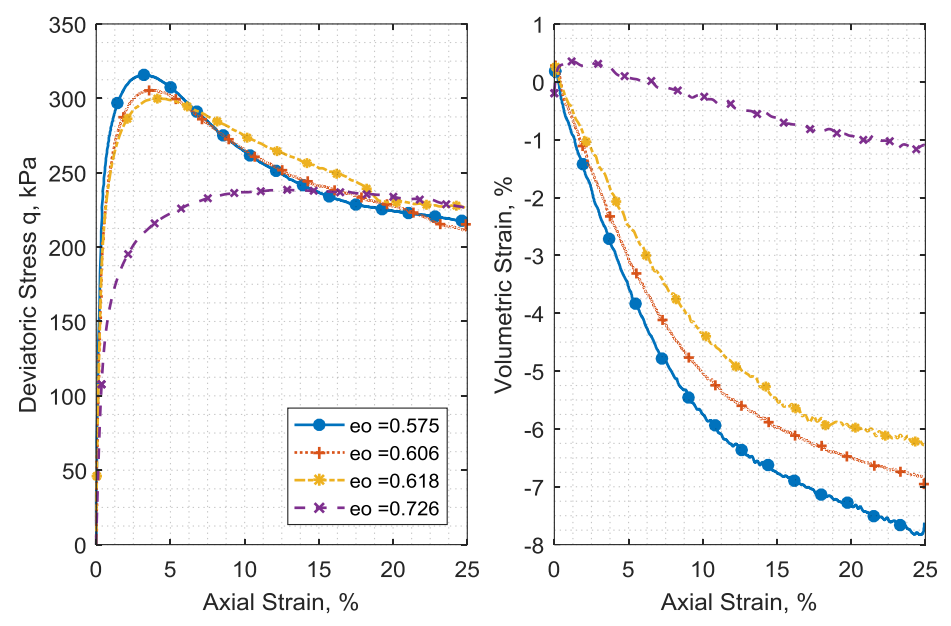


Figure 2: Drained triaxial tests on samples with different densities and similar confining stress

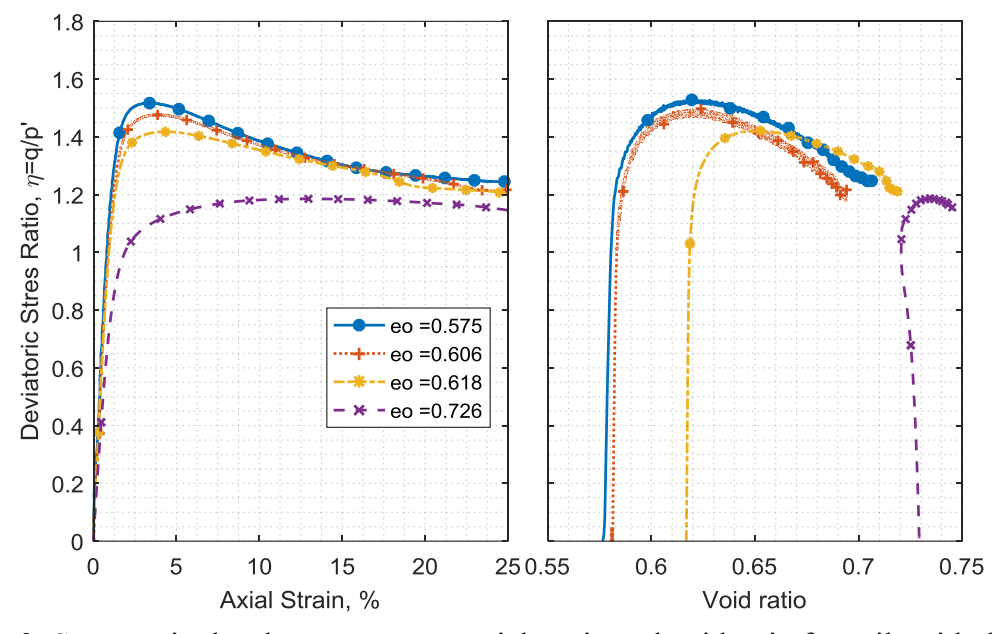


Figure 3: Stress ratio development versus axial strain and void ratio for soils with different densities

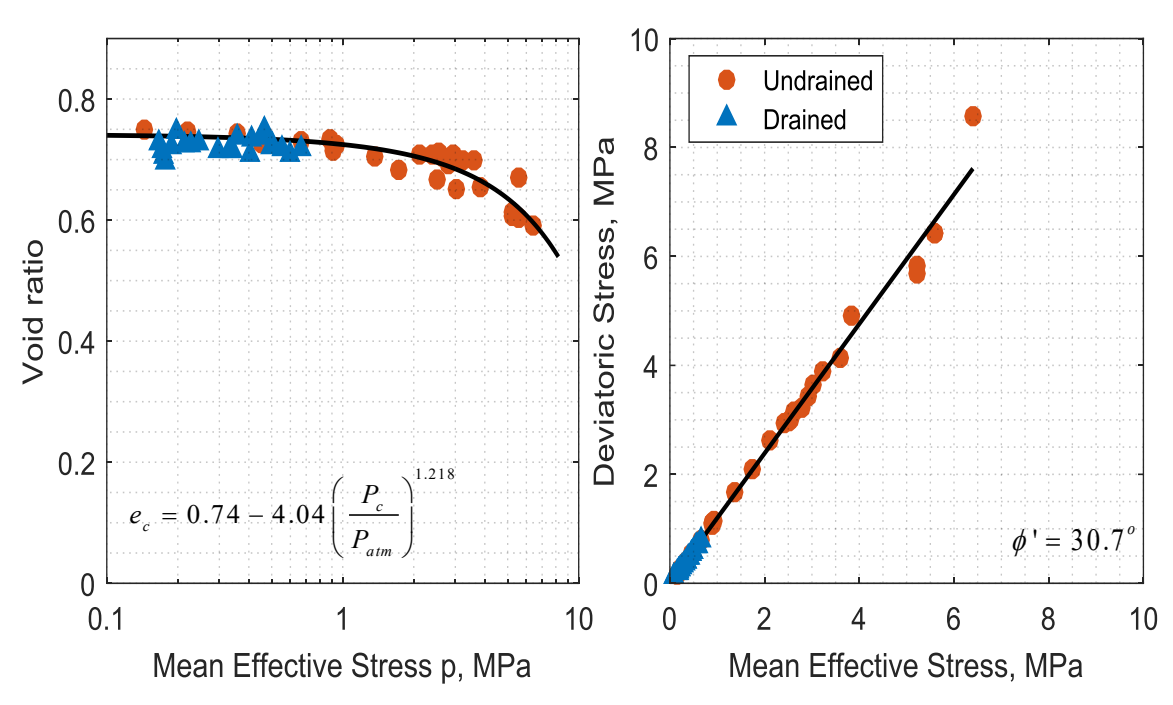


Figure 4: Critical state of undrained and drained tests prepared by the CHDP method

4. Sample Preparation and Test Setup

4.1. Triaxial Testing Equipment

Three different triaxial equipment was used in this study. The first testing equipment used was the CKC e/p cyclic triaxial testing system manufactured by C.K. Chan (Soil Engineering Equipment Co.). The setup of the machine is shown in Figure 5. It employs an electro-pneumatic system, which relies on in-house pressure for operation. Different testing conditions are permitted in this system including consolidation testing, monotonic stress/strain controlled testing, and cyclic stress/strain-controlled testing among other tests. In this study, this machine was used to perform drained monotonic compression and cyclic stress-controlled experiments. While the machine is versatile and can test the soil under different conditions, it is limited by the cell pressure capacity of 700 kPa.

A newer triaxial machine available to the authors is shown in Figure 6. This equipment applies pressure through electric pumps, and the axial force is provided by an electric motor, thus eliminating the need for compressed air. The machine is capable of running cyclic triaxial stress and strain-controlled tests. The new data acquisition system in the machine resulted in a better quality of the measured data. However, the pressure capacity for this equipment is similar to the CKC Machine. In this study, the new triaxial machine was used to perform a series of cyclic strain-controlled triaxial experiments.

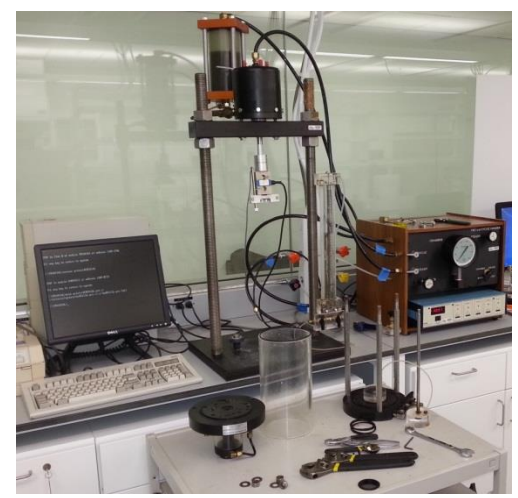


Figure 5: CKC e/p Cyclic Triaxial Testing Machine



Figure 6: Geocomp Cyclic Triaxial Machine

4.2. Cyclic Direct Simple Shear Equipment

A uniaxial direct simple shear (DSS) device, Figure 7, was used in the cyclic direct simple shear tested reported here. The DSS machine is designed to run using horizontal and vertical motors that control the displacements. Teflon coated rings are used to restrain the soil specimen laterally as shown in Figure 8. To mimic the undrained condition, the specimen height is kept constant through the test. Encoders are used for higher precision measurement of the displacements and better control during shearing. Additional bender elements are also added to the top and bottom cap to measure the shear wave velocity of the soil using an external device shown in Figure 9.

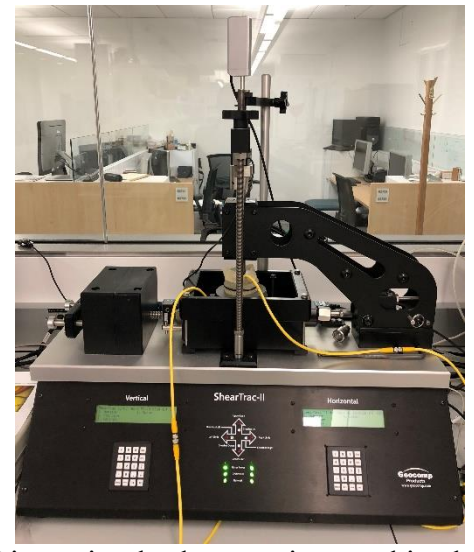


Figure 7: Direct simple shear testing machine by Geocomp

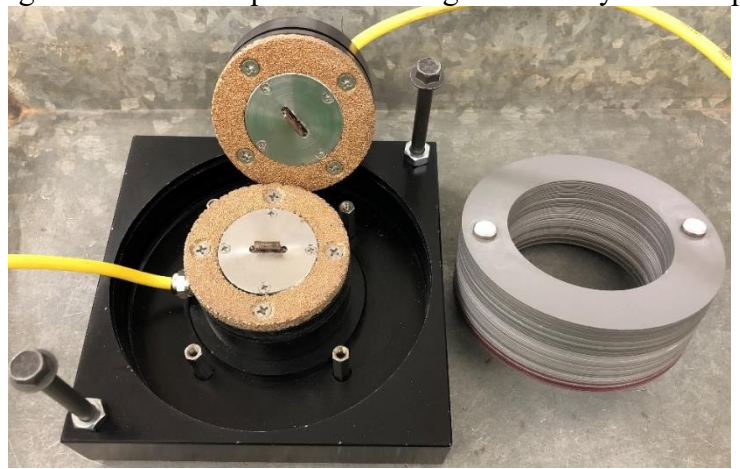


Figure 8: Top and bottom caps and Teflon rings



Figure 9: Shear wave velocity measurement device

4.3. Constant Height Dry Pluviation Method

A Constant Height Dry Pluviation method was used for the sample preparation. In this method the target dry density is achieved by pouring the sand into the mold from a specific height. In order to create a more uniform specimen, a constant height of drop between the sample surface

and hopper should be maintained. In order to produce specimens with similar fabric and consistency, three types of sand pluviators were considered. The first pluviator, Figure 10, was used for preparing specimens with void ratio of 0.515 (ρ_d=1774.2 kg/m³). The pluviator is composed of a sand hopper with a top diameter of 24 cm and total depth of 21 cm. The exit diameter of the hopper is 7.5 cm. The bottom (exit) part of the bucket is covered with a shutter plate with thirteen openings. Each opening has a diameter of 0.5 cm. the end of the pluviator has a #8 sieve with a mesh opening of 2.36 mm. The distance between the sieve and the shutter plate is 15.0 cm. The drop height of the sand (distance from the sieve to the surface of the deposited sand) is 19.8 cm. In order to control the flow rate of the sand and the uniformity of the sand placed in the pluviator, a dispersion cup hanging from the top of the pluviator is used to place the sand in the hopper with a consistent and uniform density.



Figure 10: Sample Pluviator 1

The second pluviator, Figure 11, was used for preparation of specimen with initial void ratios 0.585 (ρ_d =1665.6 kg/m³) and 0.542 (ρ_d =1712.6 kg/m³). This pluviator is composed of a hopper with the same dimensions as those of pluviator 1, i.e. with a diameter of 24.0 cm and depth of 21 cm. The distance from the bottom (exit) of the hopper to the end of the pluviator is 30 cm. The end of the pluviator has an opening of 2.0 cm and it is covered with a #8 sieve. The drop height is 2.0 cm and 4.0 cm for samples with void ratio of 0.585 and 0.542, respectively. A dispersion cup is used for sample uniformity and flow rate control.

The third pluviator is shown in Figure 12. This pluviator was designed to obtain a looser sand specimen. It consists of a tube with a diameter of 1 inch attached to a bucket at the top and covered with a #8 sieve at the bottom. In order to achieve loose samples a small dispersion cone was designed and placed right above the sieve. The function of the cone is to control the flow rate of the falling sand. In addition, it maintained the same scatter as the other two pluviators, thus creating a soil fabric that is similar to the fabrics of the specimens prepared with other pluviators.



Figure 11: Sample Pluviator 2

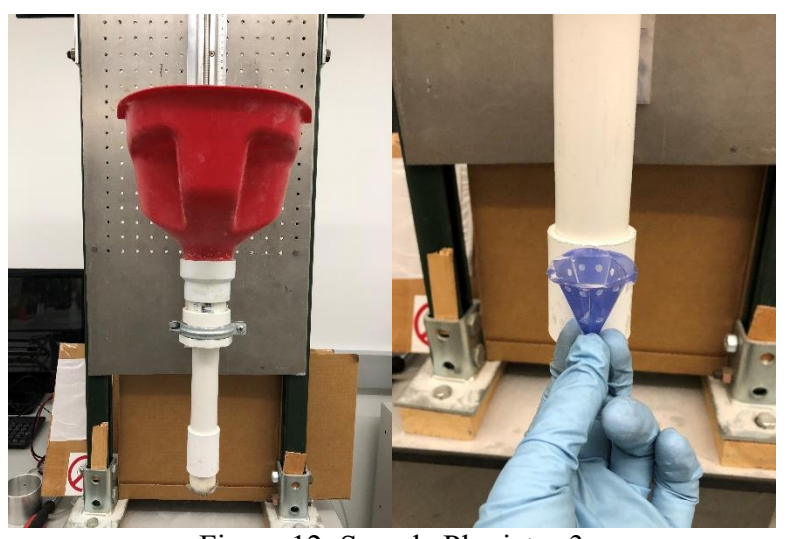


Figure 12: Sample Pluviator 3

In order to maintain a constant height of drop during the sample preparation a pluviator lift, Figure 13, was employed. The pluviator lift is composed of a support for the sample pluviator.

The support is attached to a steel frame and it is moved upwards and downwards through a threaded rod. The movement of the threaded rod is controlled by a DC motor. The speed of the motor is controlled by a power supply. During the sample preparation, the sand is gradually deposited until it flows from the surface of the mold. Afterwards the sample surface is leveled in order to ensure a consistent sample height. The excess sand is collected in the sand collector.



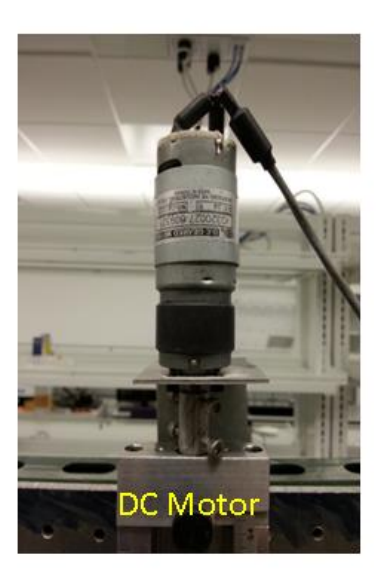




Figure 13: Pluviator Lift

5. Stress-Controlled Cyclic Triaxial Tests

Three sets of experiments were performed on the specimens with void ratios of 0.515, 0.542 and 0.585 (pd = 1744.2, 1712.6, 1665.6 kg/m3). According to the maximum and minimum void ratios accepted by LEAP, theses void ratios correspond to the relative densities of 97.5%, 87.5%, and 71.5%, respectively. The database [22,23] obtained from these tests were provided to modelers as part of the prediction exercise conducted as part of the LEAP-UCD-2017 project [11,12].

A total of 23 experiments were performed. The CHDP method was used in preparation of all the soil specimens in these tests. Table 1 shows the statistics of the measured dimensions and weights of these specimens. It is observed that the coefficient of variation for the specimen measurements was below 1%. Figures 14 to 16 show the cumulative distribution for the weight, height, and diameter of the tested specimens. The distribution of the measured data can be fitted using a normal distribution as can be seen in the figures. While Figure 14 shows the distribution

of the sample weight for each void ratio separately, Figure 15 and 16 respectively combine the height and diameter measurements of all the tested specimens.

Table 1: Statistics of the measurements of the tested soil specimens

Measurement	Mean	COV (%)
Height, mm	164.64	0.24
Diameter, mm	71.14	0.18
Weight (e ₀ =0.515), g	1142.27	0.30
Weight (e ₀ =0.547), g	1120.31	0.42
Weight (e ₀ =0.585), g	1088.95	0.51

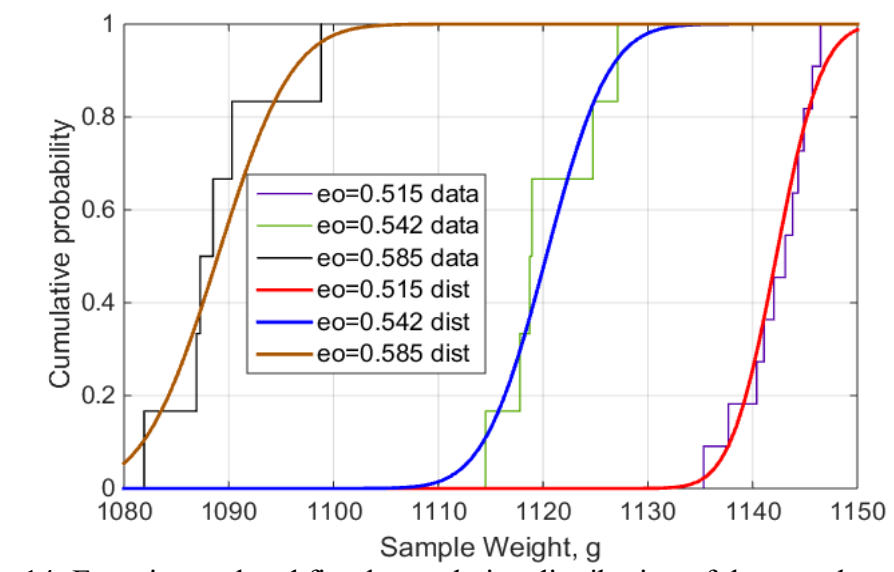


Figure 14: Experimental and fitted cumulative distribution of the sample weight data

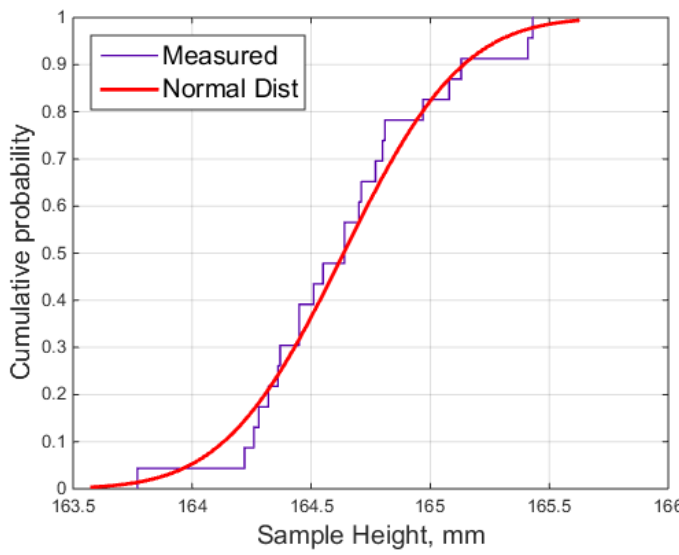


Figure 15: Experimental and fitted cumulative distribution of the sample height data

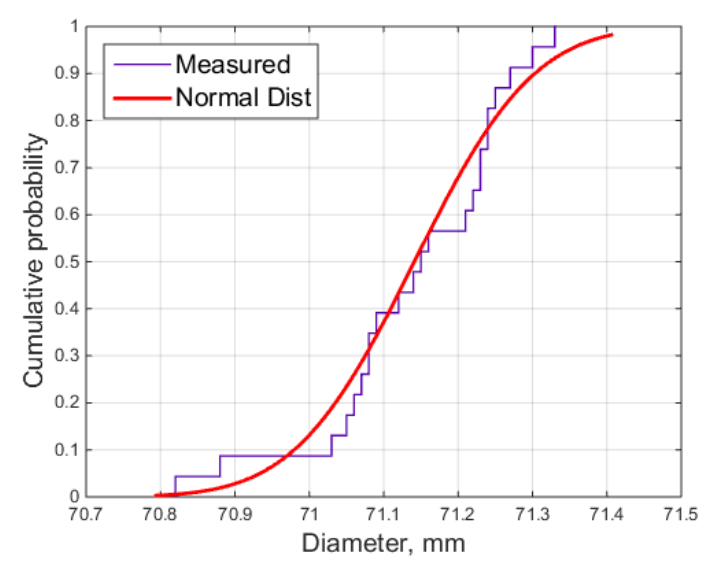


Figure 16: Experimental and fitted cumulative distribution of the sample diameter data

Figure 17 presents the results obtained from one of the cyclic triaxial tests. The tested specimen is dense with an initial void ratio of 0.515 and confining stress of 100 kPa. The specimen is subjected to cyclic shear stress with a cyclic stress ratio (CSR) of 0.325. The effective stress path, the stress-strain response, the mean effective stress vs. strain response and the excess pore pressure development are shown. It can be seen that the response of the soil specimen follows a typical cyclic mobility pattern. The liquefaction strength of the soil is measured based on the number of cycles required to achieve a certain level of shear strain. In this study, the criterion is taken to be the number of cycles to develop a single amplitude shear strain of 2.5%.

Tables 2, 4 and 6 show a summary of the experiments performed for each initial void ratio. The tables show the achieved void ratios after specimen preparation, after completion of consolidation, and just before the shearing phase. The numbers of cycles until 2.5% single amplitude of axial strain and until an excess pore pressure ratio of 1.0 is first achieved are shown. Tables 3, 5 and 7 show the statistics of the void ratios and the B values achieved. The tables show that the sample was consistently saturated to a B > 0.95 and the coefficient of variation of the achieved void ratio was less than 1.3%. Figure 18 shows the liquefaction strength curves obtained for the three soil densities tested.

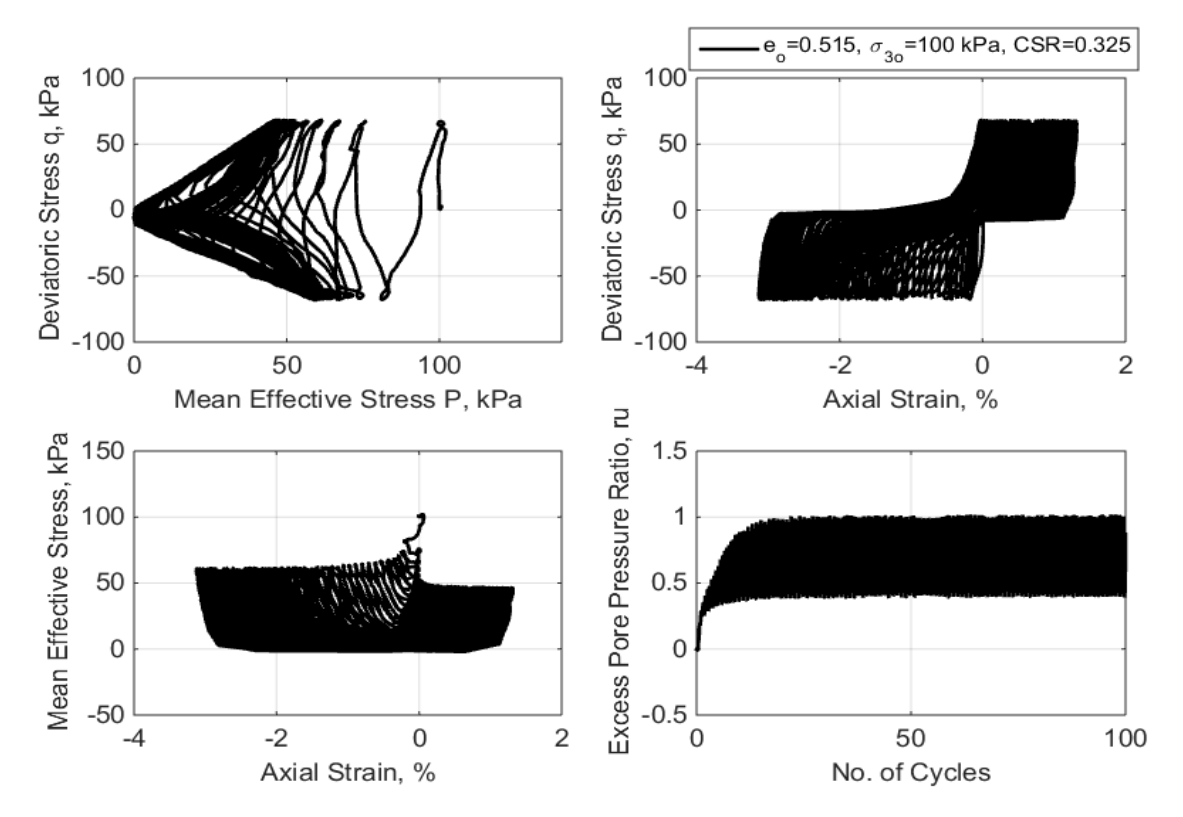


Figure 17: Triaxial experiment results of Ottawa F65 sand specimen with a void ratio of 0.515 and CSR of 0.325

Table 2: Summary of experiments on specimens with e₀=0.515

e_0 =0.515 - ρ_d =1744.2 kg/m ³									
Date	ea	eo	В	es	CSR	2.5% s.a.	$r_{\rm u} = 1.0$		
10/10/2016	0.522	0.515	0.971	0.499	0.600	14	15.53		
10/6/2016	0.526	0.522	0.953	0.506	0.500	17	26		
10/7/2016	0.517	0.512	0.977	0.497	0.450	19	15.55		
9/16/2016	0.520	0.515	0.962	0.500	0.375	26	25		
9/27/2016	0.518	0.514	0.952	0.501	0.365	29	16		
9/30/2016	0.512	0.507	0.959	0.494	0.325	41	18		
9/22/2016	0.518	0.514	0.950	0.502	0.315	46	37		
9/28/2016	0.521	0.516	0.951	0.500	0.300	48	31		
9/13/2016	0.522	0.517	0.961	0.505	0.275	60	35		
9/29/2016	0.520	0.515	0.959	0.503	0.265	70	45		
10/12/2016	0.517	0.513	0.951	0.501	0.225	191	140		

Table 3: Statistics of experiments on specimens with $e_0 = 0.515$

	ea	e _o	В	e_s
Mean	0.519	0.515	0.959	0.501
SD	0.004	0.004	0.009	0.003
COV (%)	0.696	0.703	0.918	0.681

Table 4: Summary of experiments on specimens with e_0 = 0.542

$e_o = 0.542 - \rho_d = 1712.6 \text{ kg/m}^3$										
Date	ea	e _o	В	e_{s}	2.5% s.a.	r _u =1.0	CSR			
11/20/2016	0.556	0.550	0.956	0.539	16	12	0.28			
11/18/2016	0.545	0.540	0.96	0.529	18	16	0.24			
11/16/2016	0.540	0.535	0.958	0.523	22	14	0.22			
11/16/2016	0.544	0.538	0.973	0.527	28	25	0.21			
11/16/2016	0.555	0.550	0.971	0.533	41	36	0.2			
11/21/2016	0.544	0.538	0.958	0.524	50	41	0.19			

Table 5: Statistics of experiments on specimens with $e_0 = 0.542$

	ea	eo	В	e_s
Mean	0.547	0.542	0.963	0.529
SD	0.007	0.007	0.007	0.006
COV (%)	1.199	1.204	0.765	1.136

Table 6: Summary of experiments on specimens with $e_0 = 0.585$

$e_0=0.585$; $\rho_d=1665.6 \text{ kg/m}^3$										
Date	e_a	eo	В	es	CSR	2.5% s.a.	ru=1.0			
11/10/2016	0.589	0.581	0.955	0.57	0.2	9	9			
11/1/2016	0.592	0.584	0.963	0.562	0.17	15	13			
11/2/2016	0.592	0.587	0.953	0.567	0.16	17	16			
11/4/2016	0.581	0.575	0.955	0.557	0.14	33	31			
11/7/2016	0.605	0.598	0.958	0.581	0.12	59	58			
11/14/2016	0.588	0.583	0.954	0.566	0.10	188	186			

Table 7: Statistics of experiments on specimens with e₀=0.585

	ea	eo	В	es
Mean	0.591	0.585	0.956	0.567
SD	0.008	0.008	0.004	0.008
COV (%)	1.334	1.310	0.384	1.434

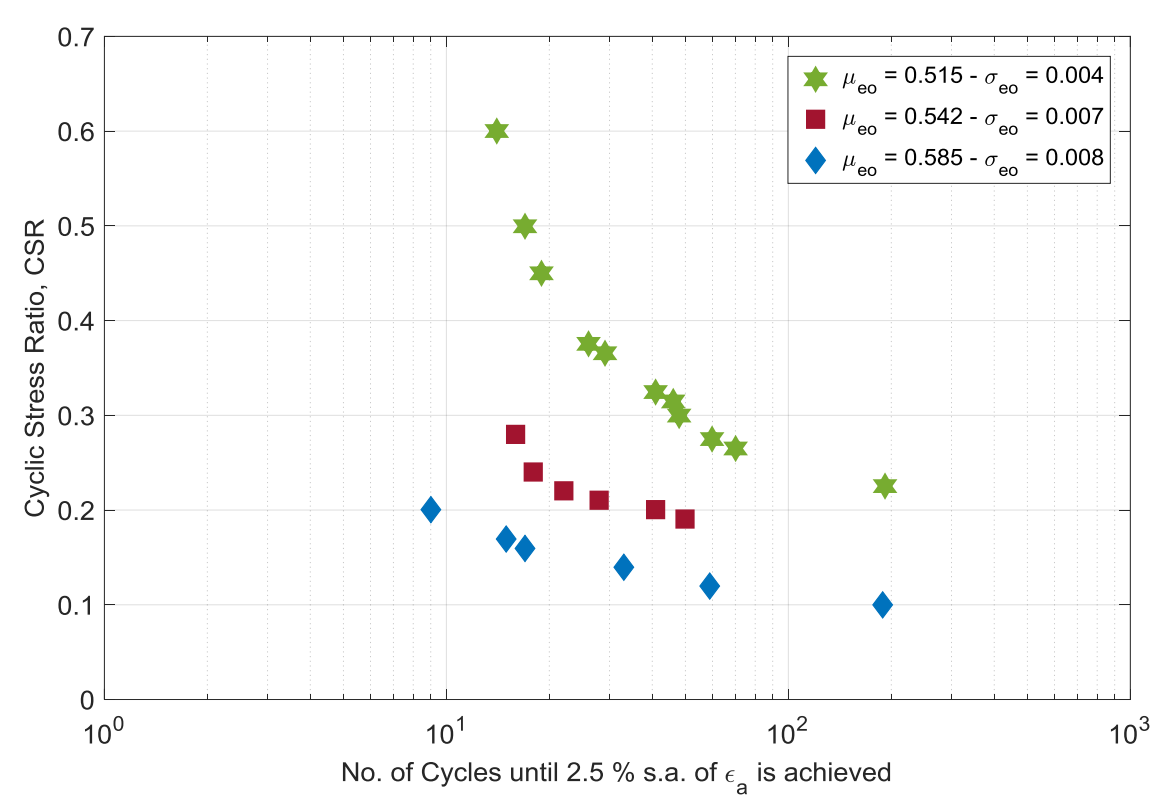


Figure 18: Liquefaction Strength Curve for Ottawa F65 Sand

While the curves shown in Figure 18 have been used to describe the liquefaction strength of the soil, they only represent a single snapshot of the soil response at the end of the tests. In order to gain more insight into the progression of the soil response, additional information was obtained by counting the number of cycles it took to reach different levels of shear strain. Figures 19 to 21 show the strength curves corresponding to a range of strains (0.5% to 2.5%) for the soil specimens with initial void ratios of 0.585, 0.542 and 0.515, respectively. It can be seen that as the soil density increases the number of shear cycles required to move from one shear strain level to the next level increases.

It is also useful to observe the progression of the soil response in terms of excess pore water pressure ratio, r_u . Figures 22 to 24 show the variation of a number of shear stress cycles required to reach certain levels of r_u (in the range of 0.7 to 0.99) for the samples with initial void ratios of 0.585, 0.542 and 0.515, respectively. It is observed that as the soil density increases the number of shear stress cycles required to generate certain levels of excess pore pressure ratio increases.

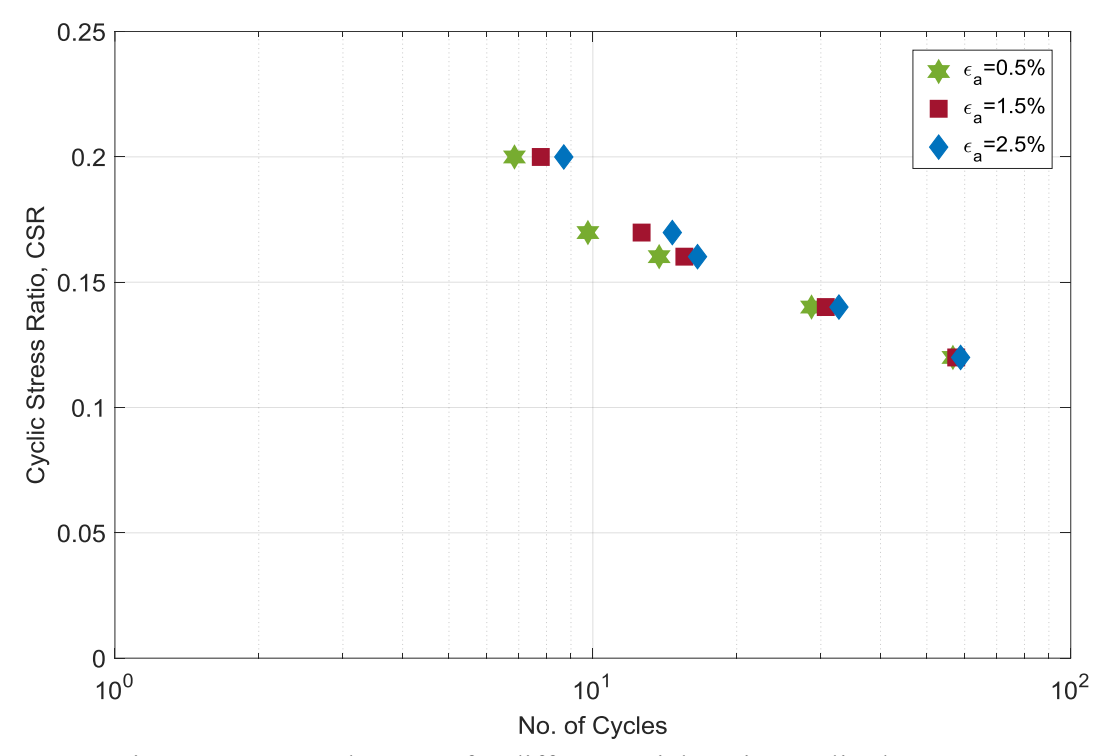


Figure 19: Strength curves for different axial strain amplitudes - $e_0 = 0.585$

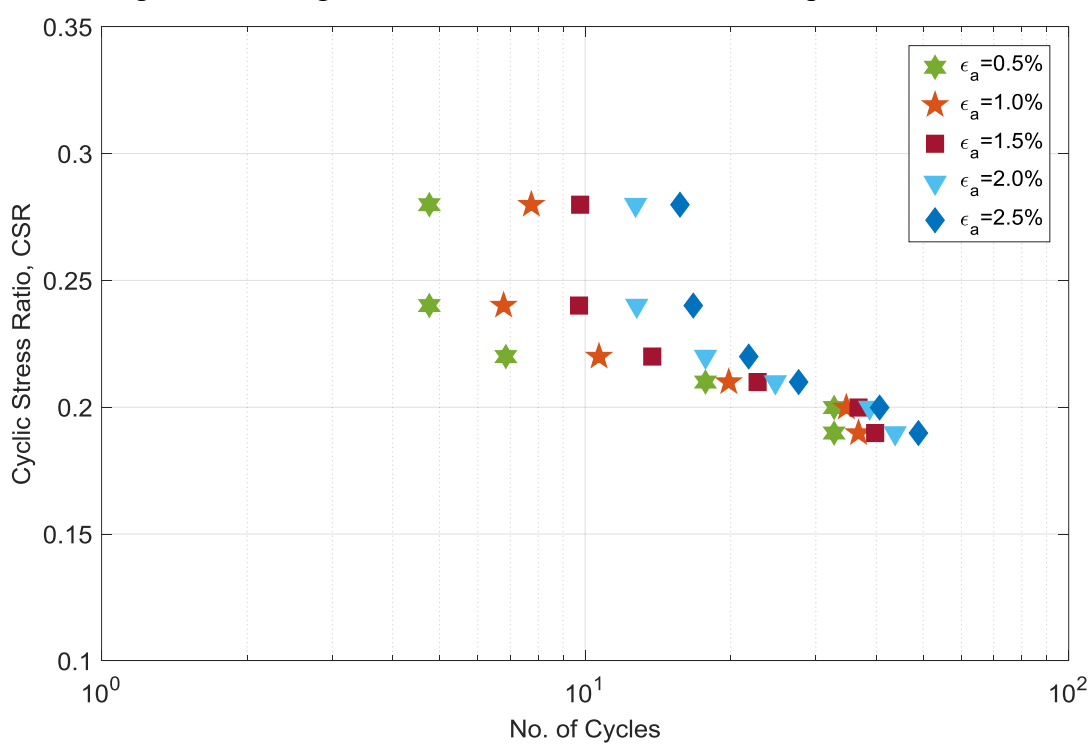


Figure 20: Strength curves for different axial strain amplitudes - $e_0 = 0.542$

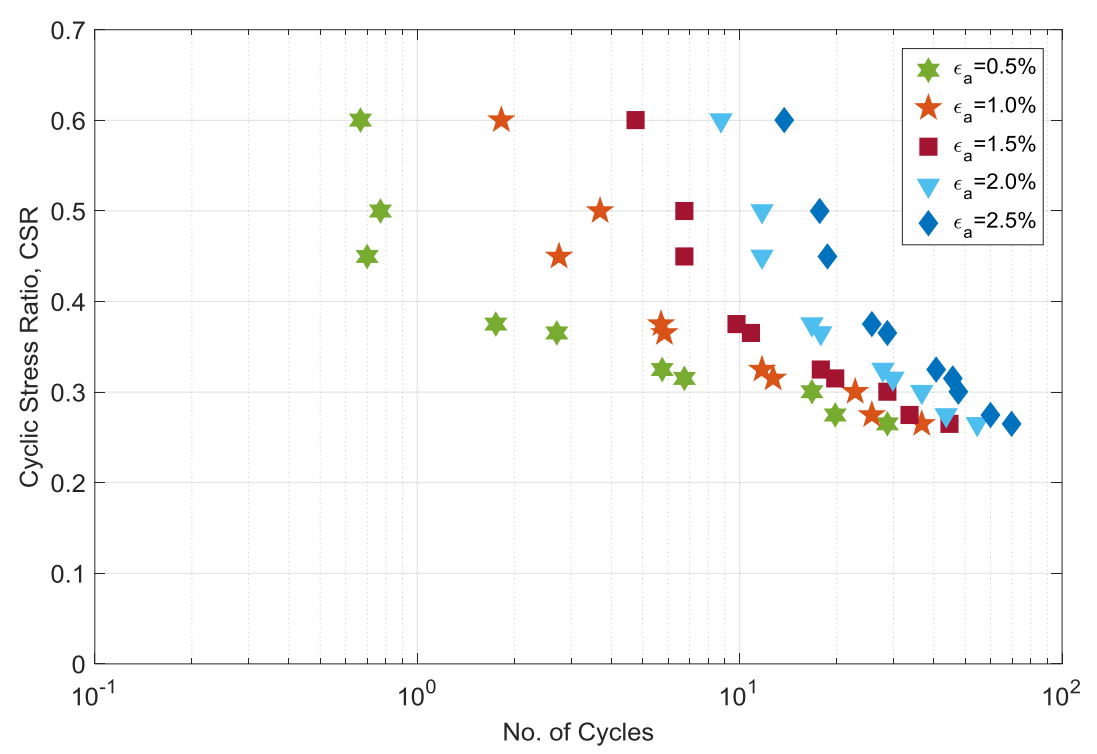


Figure 21: Strength curves for different axial strain amplitudes - $e_{\text{o}} = 0.515$

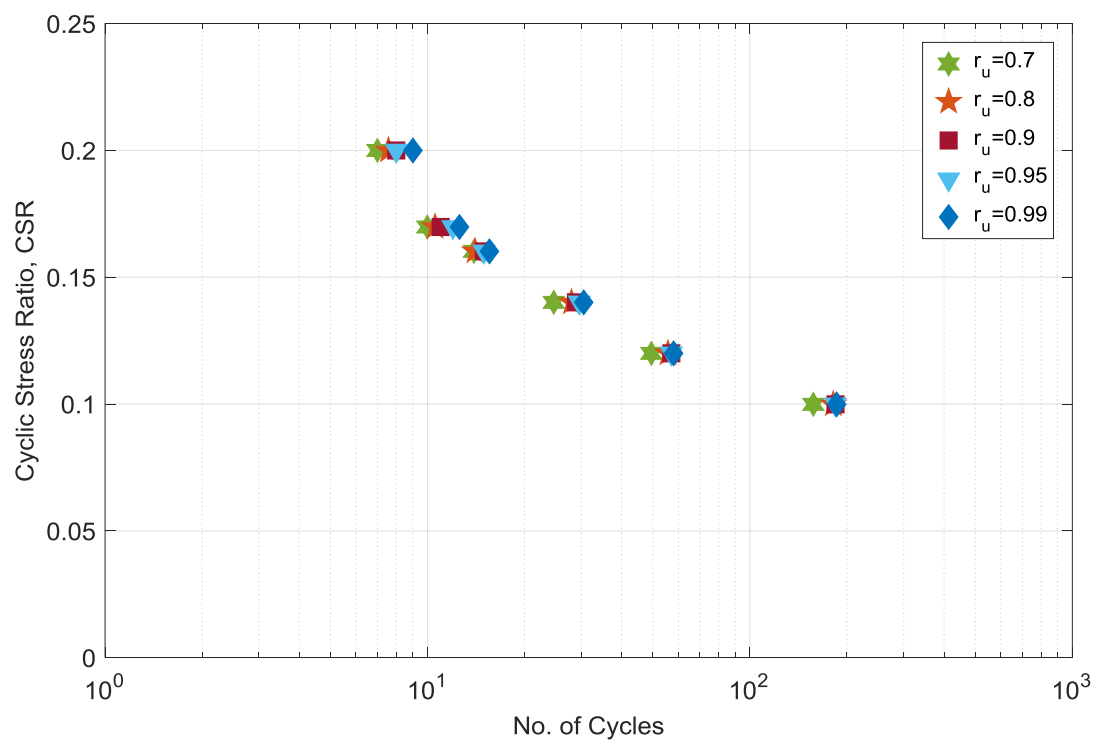


Figure 22: Strength curves for different excess pore pressure ratios - $e_0 = 0.585$

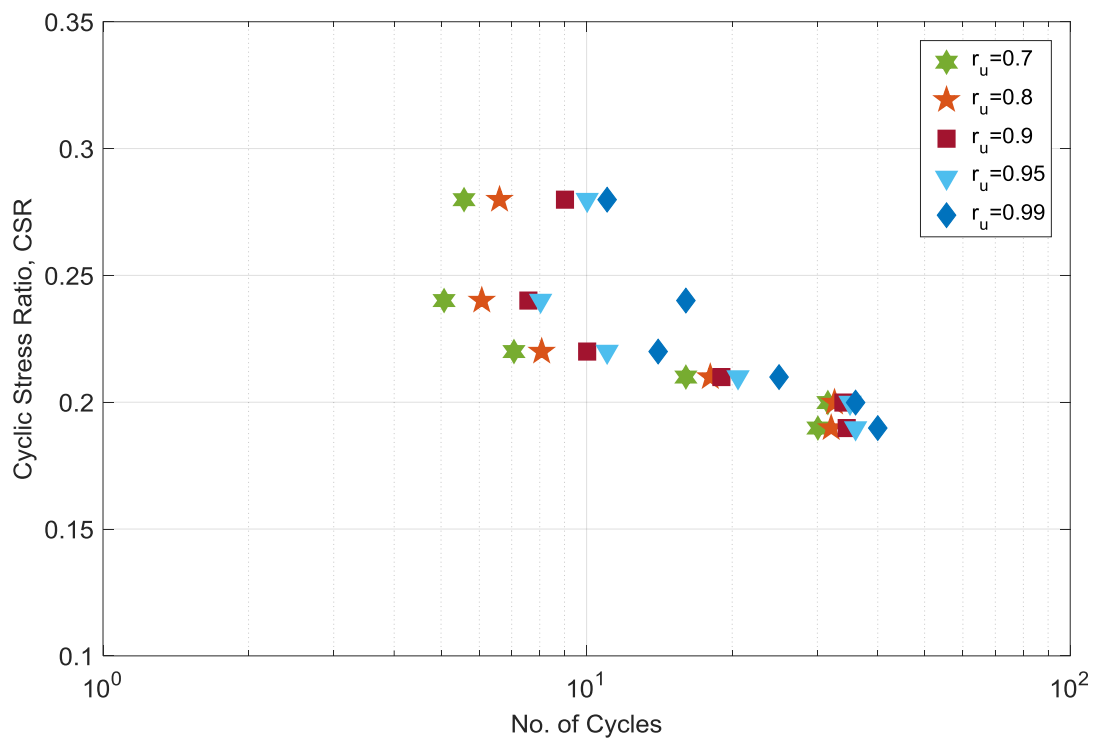


Figure 23: Strength curves for different excess pore pressure ratios - $e_o = 0.542$

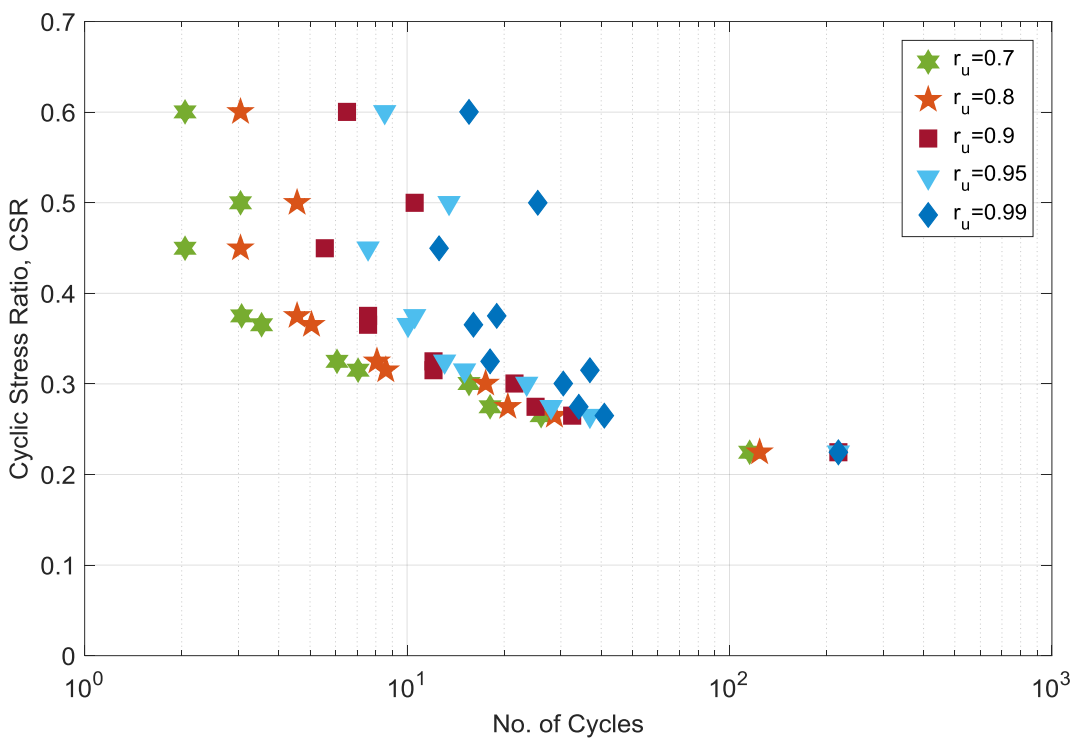


Figure 24: Strength curves for different excess pore pressure ratios - $e_o = 0.515$

6. Strain-Controlled Cyclic Triaxial Tests

Three sets of strain-controlled cyclic triaxial experiments were conducted with the following void ratios of 0.576, 0.608 and 0.668 (ρ_d = 1681.65, 1648.35, 1588.4 kg/m³). According to the maximum and minimum void ratios accepted by LEAP, the relative densities are 75.6%, 63.8%, and 40.0% for the samples with void ratios of 0.576, 0.608 and 0.668, respectively.

Thirty seven experiments were performed in total. The test specimens were prepared by the CHDP method. The statistics obtained on the measurements of the sample dimensions and weight are shown in

Table 8. It can be seen from the results in the table that the coefficient of variations for the specimen measurements were around 1%. Figures 25 to 27 show the cumulative distribution for the sample weight, height, and diameter. The distribution of the measured data can be fitted using a normal distribution as can be seen in the figures. While Figure 25 shows the distribution of the sample weight for each void ratio separately, Figures 26 and 27 combine the measurements of all the tested specimens for the sample height and diameter respectively.

Table 8: Statistics of Soil Specimens

Tuest of a tunishes of a circle approximation						
Measurement	Mean	COV (%)				
Height, mm	159.63	0.41				
Diameter, mm	70.92	0.17				
Weight (e ₀ =0.576), g	1057.97	0.40				
Weight (e ₀ =0.608), g	1040.44	0.68				
Weight (e ₀ =0.668), g	991.51	1.18				

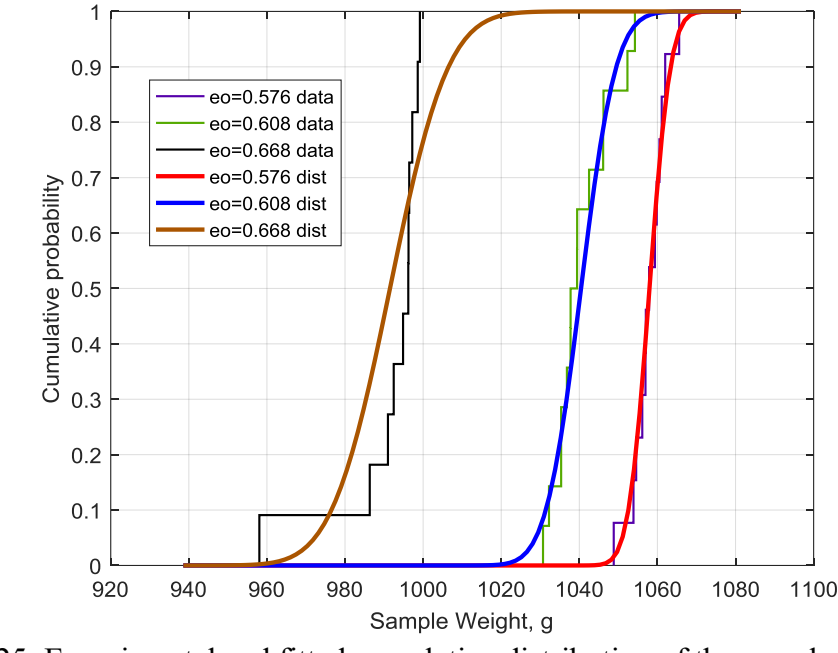


Figure 25: Experimental and fitted cumulative distribution of the sample weight data

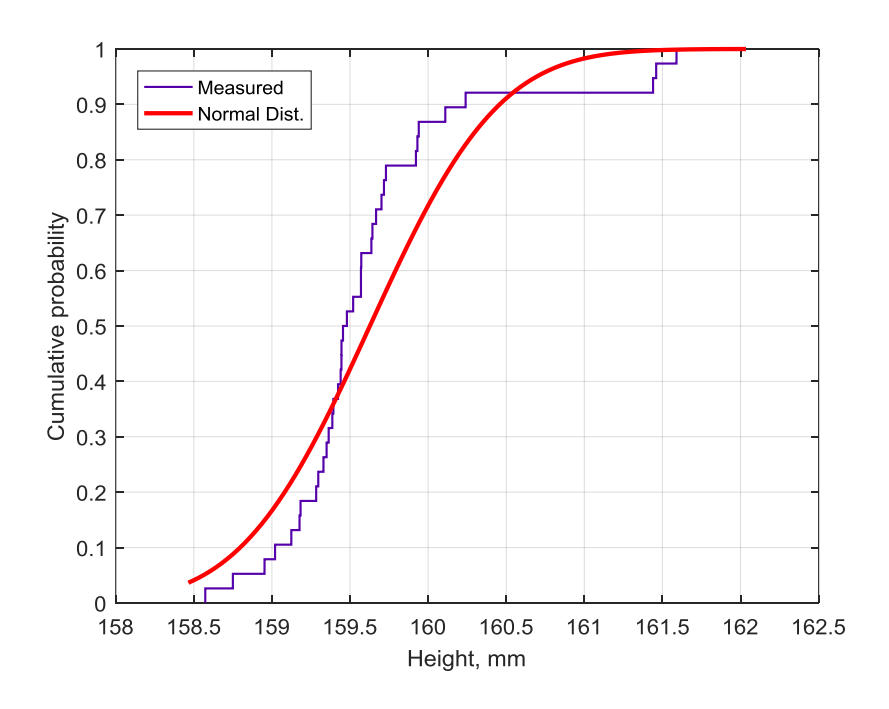


Figure 26: Experimental and fitted cumulative distribution of the sample height data

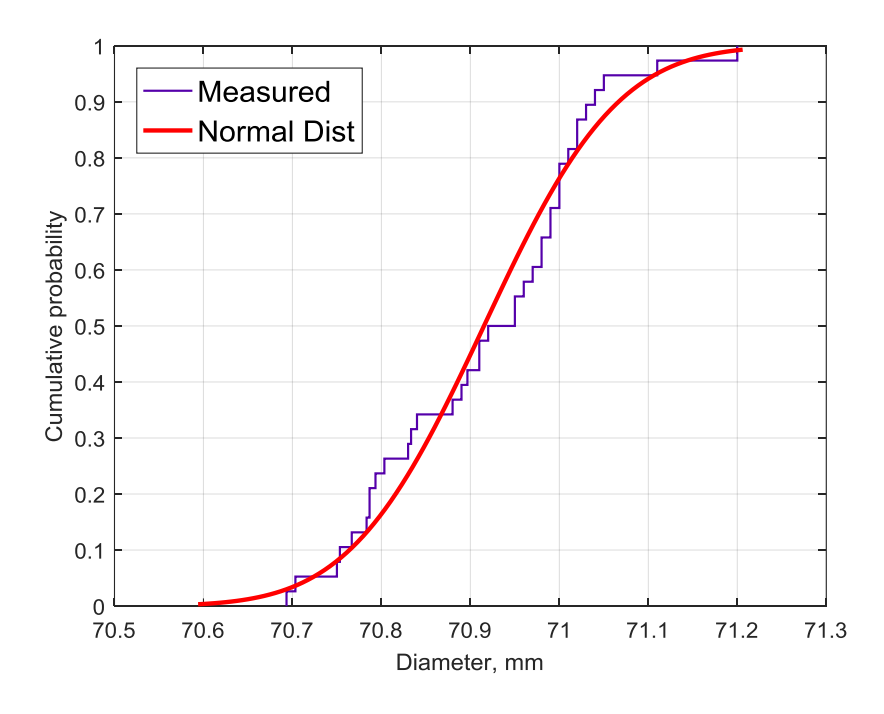


Figure 27: Experimental and fitted cumulative distribution of the sample diameter data

Figure 28 shows the results obtained from one of the strain-controlled cyclic triaxial tests on a medium dense sample with an initial void ratio of 0.608 and confining stress of 100 kPa. The specimen was sheared to a constant cyclic strain with a cyclic strain amplitude (CSA) of 0.22%. In a similar fashion to the cyclic stress-controlled tests, the plot shows the effective stress path, the stress-strain response, the mean effective stress vs. strain response and the excess pore pressure

development. Because of the dilative nature of this medium dense specimen, it can be seen that a negative excess pore pressure is generated in the first cycle and upon load reversal, significant positive excess pore pressure is developed. The peak shear stress generated in each cycle decreases with a constant slope. The largest shear stress ratio on the compression side has a value of 1.24 which corresponds to a mobilized friction angle of 30.9° (which is equal to the critical state friction angle). The largest shear stress ratio on the extension side is about 0.67 which corresponds to the mobilized friction angle of 22.2°.

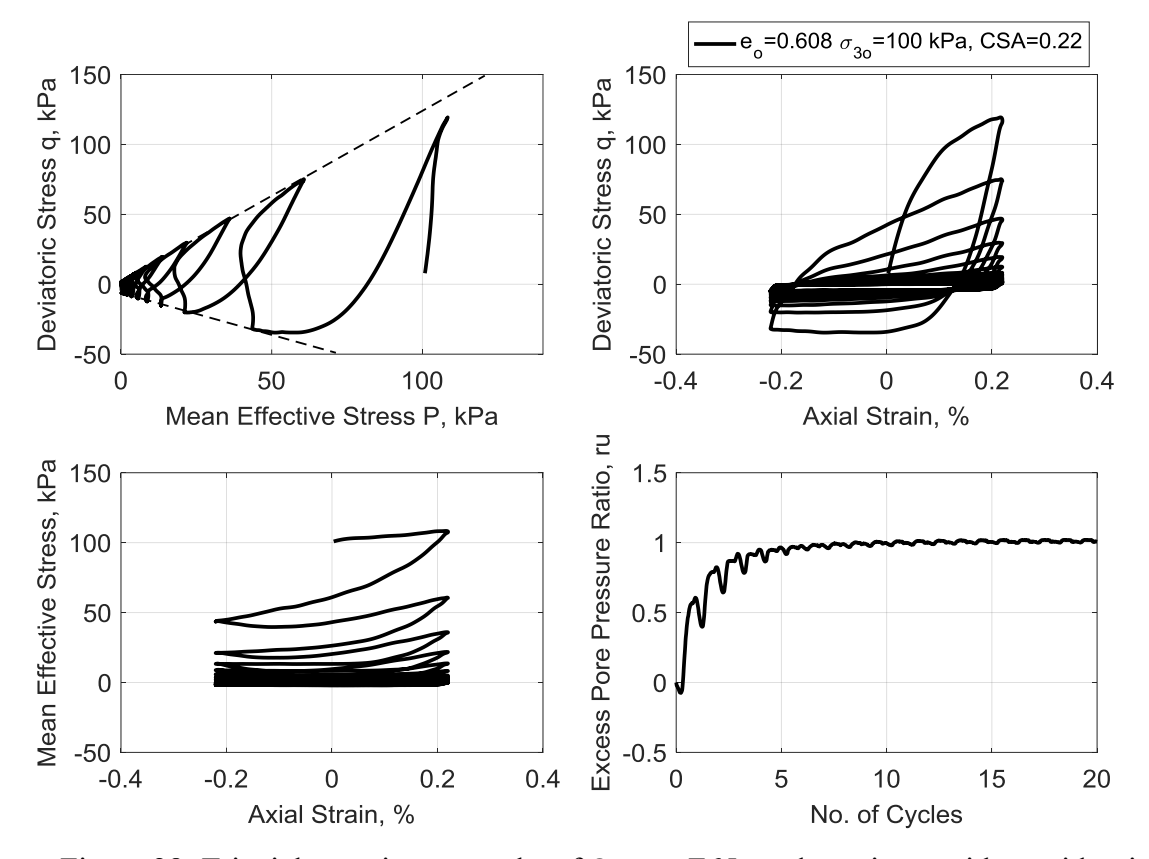


Figure 28: Triaxial experiment results of Ottawa F65 sand specimen with a void ratio of 0.608 and CSA of 0.22%

While highly consistent sample preparation was facilitated by using the CHDP method, the consistency and repeatability of the soil response was evaluated through test repetition. Figure 29 shows the results of two tests performed on the samples prepared with the same density and subjected to the same CSA. The soil specimen has a void ratio of 0.576 and the CSA applied is 0.1%. The repeatability of the soil response observed in Figure 29 provides additional confirmation of the sample preparation technique.

In all the conducted strain-controlled tests, the soil is assumed to reach liquefaction when the excess pore water pressure developed is equivalent to the initial mean effective stress. In this work, we look for the number of cycles required to reach an excess pore pressure ratio, r_u , of 0.95. Tables 9, 10 and 11 summarize the experiments performed for each initial void ratio. The tables

show the achieved void ratios of the soil specimen after preparation and after consolidation of the test specimens. Figure 30 shows the liquefaction strength curves obtained for the three soil densities tested.

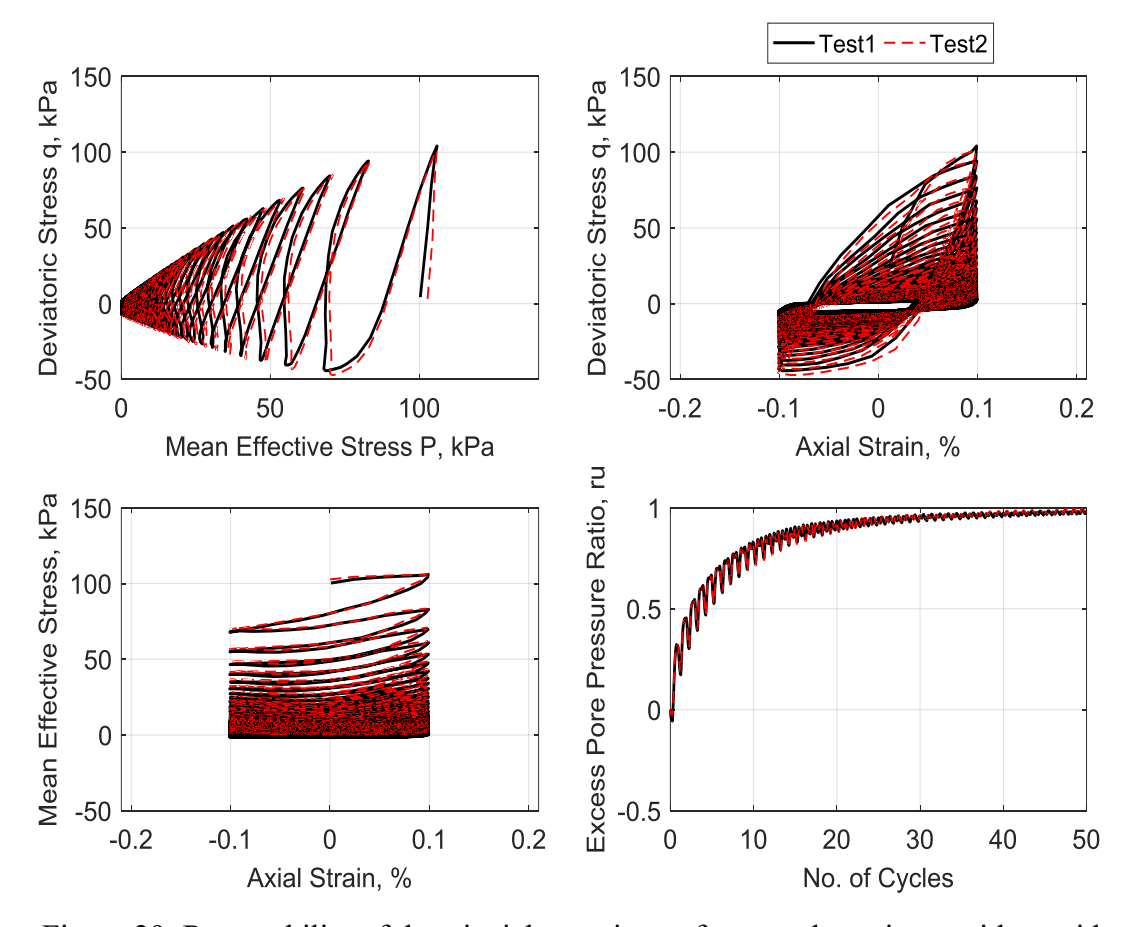


Figure 29: Repeatability of the triaxial experiment for a sand specimen with a void ratio of 0.576 and CSA of 0.1%

Table 9: Summary of experiments on specimens with eo = 0.668

	$eo=0.668 - \rho_d = 1588.4 \text{ kg/m}^3$								
Date	ea	eo	$\rho_d (kg/m3)$	CSR (%)	nCyc ru=0.95				
7/21/2017	0.672	0.667	1589.91	0.140	3.89				
7/20/2017	0.675	0.671	1585.63	0.125	4.91				
7/19/2017	0.675	0.669	1588.09	0.100	7.03				
7/20/2017	0.677	0.671	1585.84	0.080	8.92				
7/21/2017	0.669	0.664	1592.18	0.060	13.96				
7/25/2017	0.672	0.668	1589.19	0.055	25.96				
7/26/2017	0.672	0.669	1587.92	0.055	26.35				
7/24/2017	0.671	0.667	1589.68	0.050	27.01				
7/24/2017	0.672	0.668	1588.39	0.045	28.01				
7/25/2017	0.6732	0.6696	1587.19	0.040	67.34				

Table 10: Summary of experiments on specimen with eo = 0.608

$eo=0.608 - \rho_d = 1648.35 \text{ kg/m}^3$								
Date	ea	eo	$\rho_d \text{ (kg/m}^3)$	CSR (%)	nCyc ru=0.95			
7/18/2017	0.610	0.606	1650.14	0.220	3.90			
7/17/2017	0.606	0.603	1653.21	0.200	4.87			
7/17/2017	0.612	0.608	1647.95	0.165	6.90			
6/22/2017	0.610	0.607	1649.37	0.125	10.00			
5/9/2017	0.620	0.616	1639.49	0.110	11.00			
4/24/2017	0.613	0.607	1648.75	0.100	14.00			
5/8/2017	0.615	0.611	1644.72	0.090	18.00			
5/4/2017	0.619	0.616	1639.53	0.080	24.00			
6/20/2017	0.609	0.605	1650.70	0.075	27.00			
6/20/2017	0.599	0.595	1661.02	0.070	40.00			
6/22/2017	0.608	0.605	1651.39	0.065	49.00			
5/5/2017	0.625	0.622	1633.52	0.060	56.00			
6/19/2017	0.609	0.606	1649.96	0.055	58.00			
6/21/2017	0.602	0.599	1657.18	0.050	97.00			

Table 11: Summary of experiments on specimen with eo = 0.576

			1	1						
	$eo=0.576 - \rho_d = 1681.65 \text{ kg/m}^3$									
Date	ea	eo	$\rho_d \text{ (kg/m}^3)$	CSR (%)	nCyc ru=0.95					
7/14/2017	0.575	0.572	1686.17	0.300	3.92					
7/14/2017	0.577	0.574	1683.34	0.250	4.89					
7/12/2017	0.578	0.575	1682.60	0.200	8.00					
7/12/2017	0.574	0.571	1686.62	0.150	12.00					
6/29/2017	0.582	0.579	1678.38	0.110	19.00					
6/27/2017	0.579	0.575	1682.11	0.100	21.00					
7/11/2017	0.582	0.579	1678.07	0.100	21.00					
7/7/2017	0.581	0.577	1680.30	0.095	27.00					
7/5/2017	0.582	0.579	1678.05	0.090	34.00					
6/27/2017	0.581	0.578	1679.12	0.080	47.00					
7/6/2017	0.583	0.576	1681.47	0.065	73.00					
7/5/2017	0.585	0.574	1684.13	0.060	79.00					
7/13/2017	0.580	0.576	1681.04	0.050	91.00					

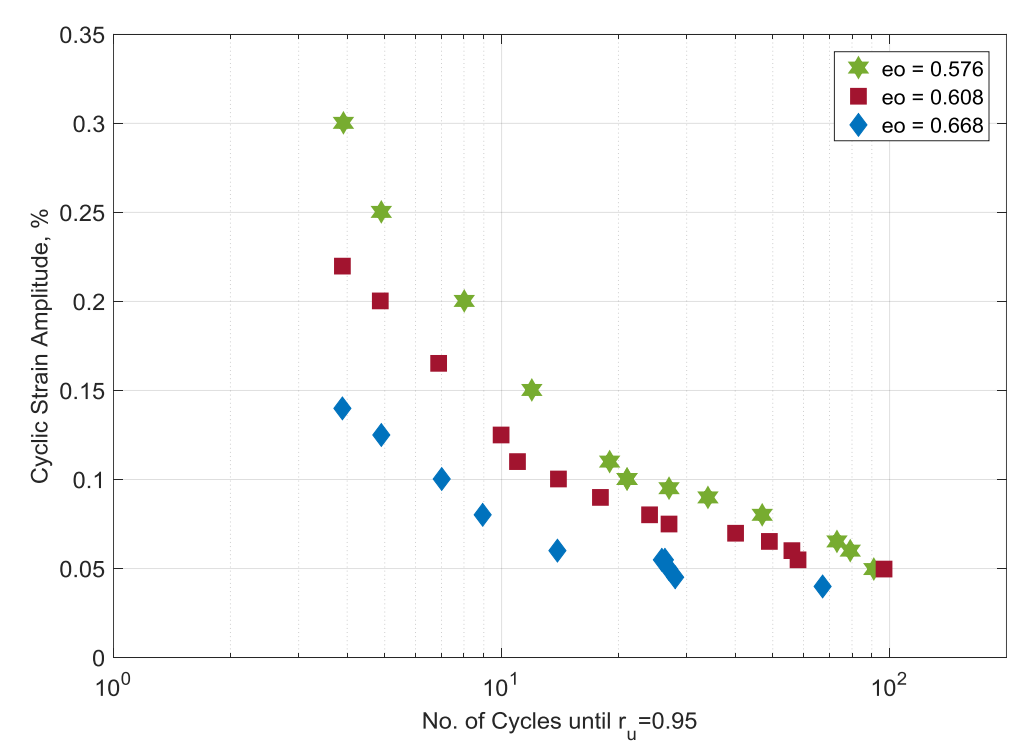


Figure 30: Liquefaction Strength Curve

The progression of the soil response in terms of the development of excess pore water pressure ratio, r_u , with the number of cycles is also an important aspect that can be used for evaluation and calibration of soil constitutive models. Figures 31 to 33 show the variation of the number of shear stress cycles required to reach certain levels of r_u (in the range of 0.7 to 0.95) for the samples with initial void ratios of 0.576, 0.608 and 0.668, respectively.

Figures 34 to 36 show the excess pore pressure generated at a different number of cycles (3, 5, 7, 10, and 15) versus the axial strain for the specimens with initial void ratios of 0.576, 0.608 and 0.668, respectively. Figures 37 to 39 compare the excess pore pressure ratio versus CSA for the three different soil densities at 5, 10 and 15 cycles respectively. As an alternative to the liquefaction strength curves, these plots show how the rate of excess pore pressure generation changes with the increase in the cyclic strain amplitudes and soil densities.

The liquefaction strength of the soil obtained from these tests are compared to data available in the literature [24] in Figure 40. Badanagki [24] performed a series of strain-controlled tests on Ottawa F65 sand with various densities that was used for calibration of constitutive models for sands purposes [25]. It can be seen that there is a good agreement between the two sets of results.

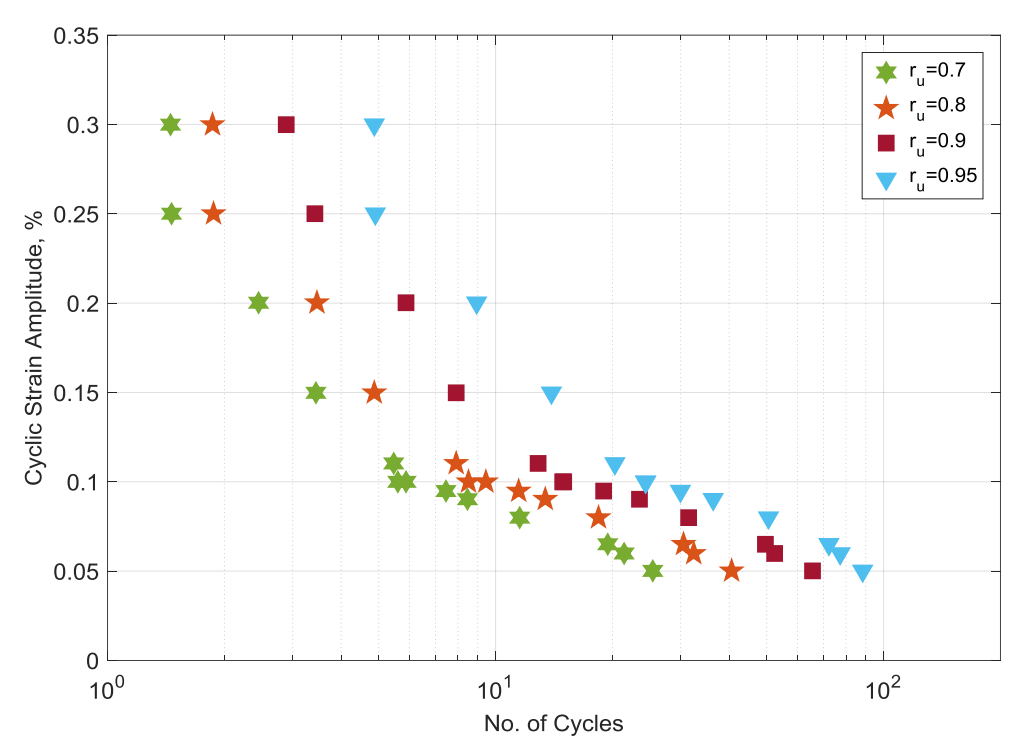


Figure 31: Strength curves for different excess pore pressure ratios - $e_0 = 0.576$

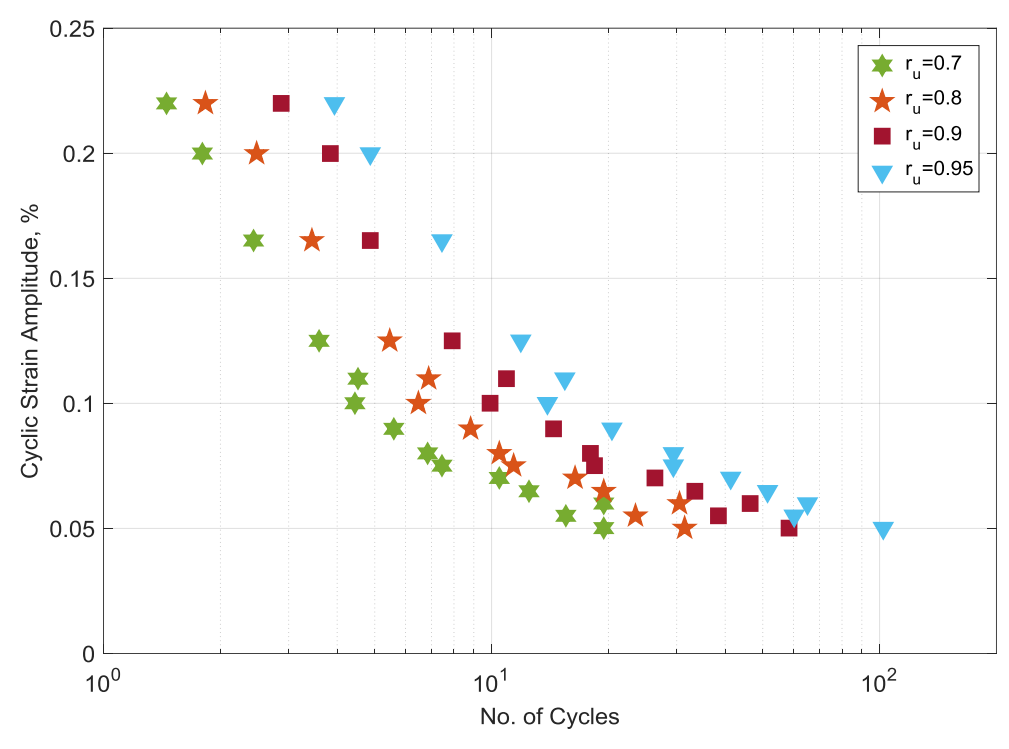


Figure 32: Strength curves for different excess pore pressure ratios - $e_0 = 0.608$

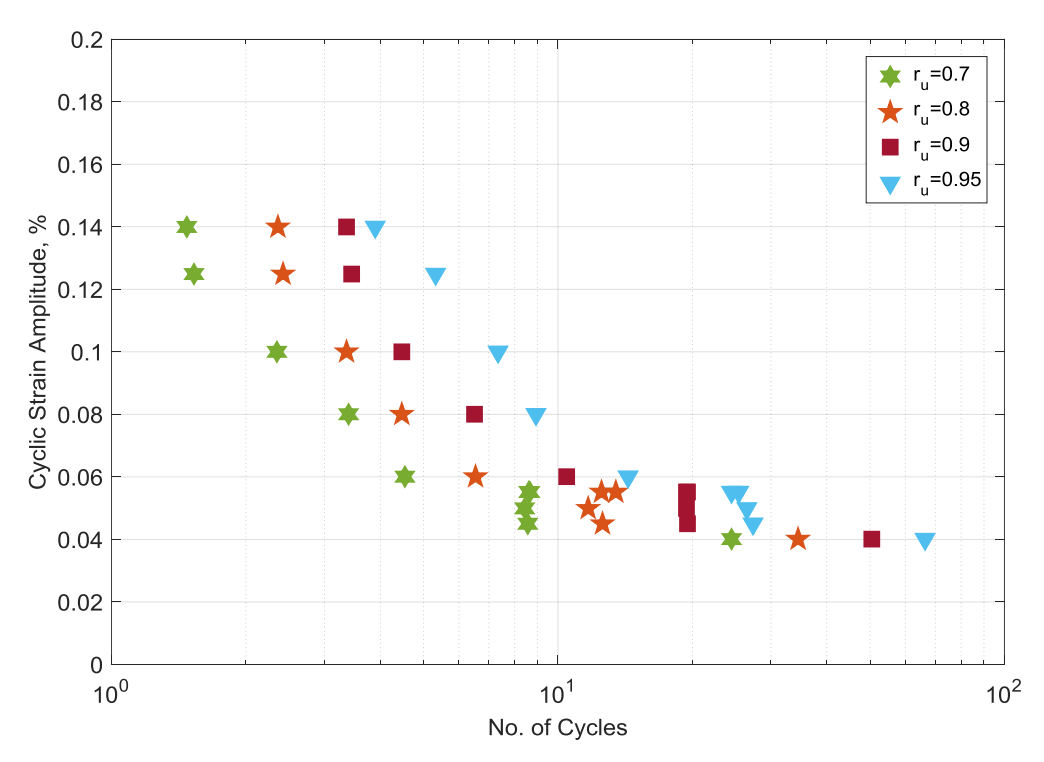


Figure 33: Strength curves for different excess pore pressure ratios - $e_0 = 0.608$

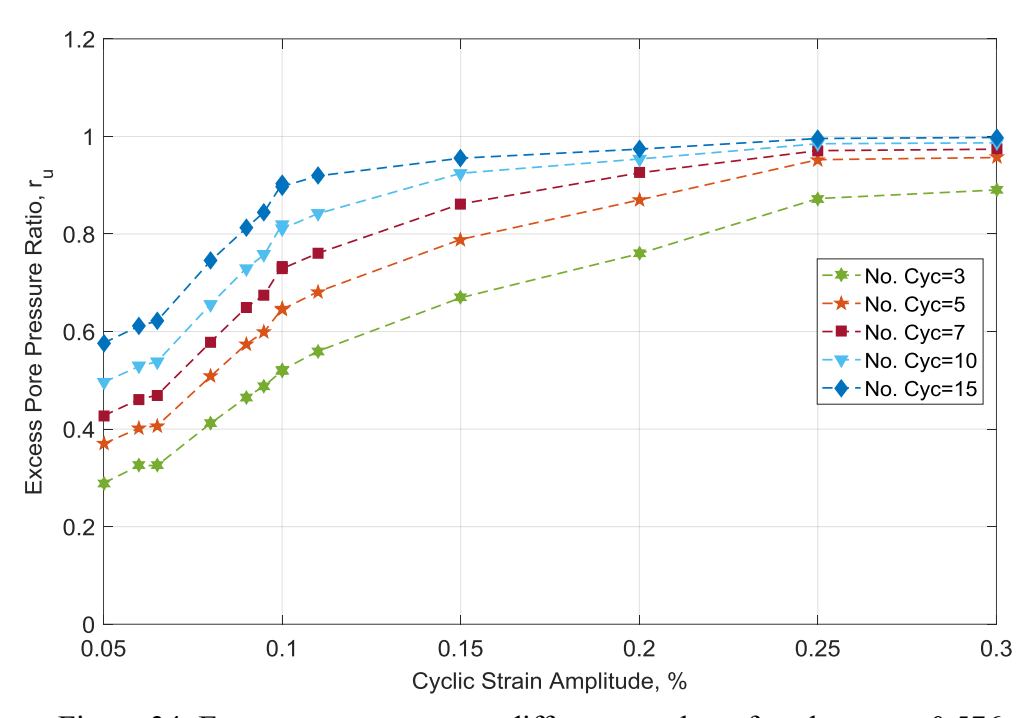


Figure 34: Excess pore pressure at different number of cycles - $e_o = 0.576$

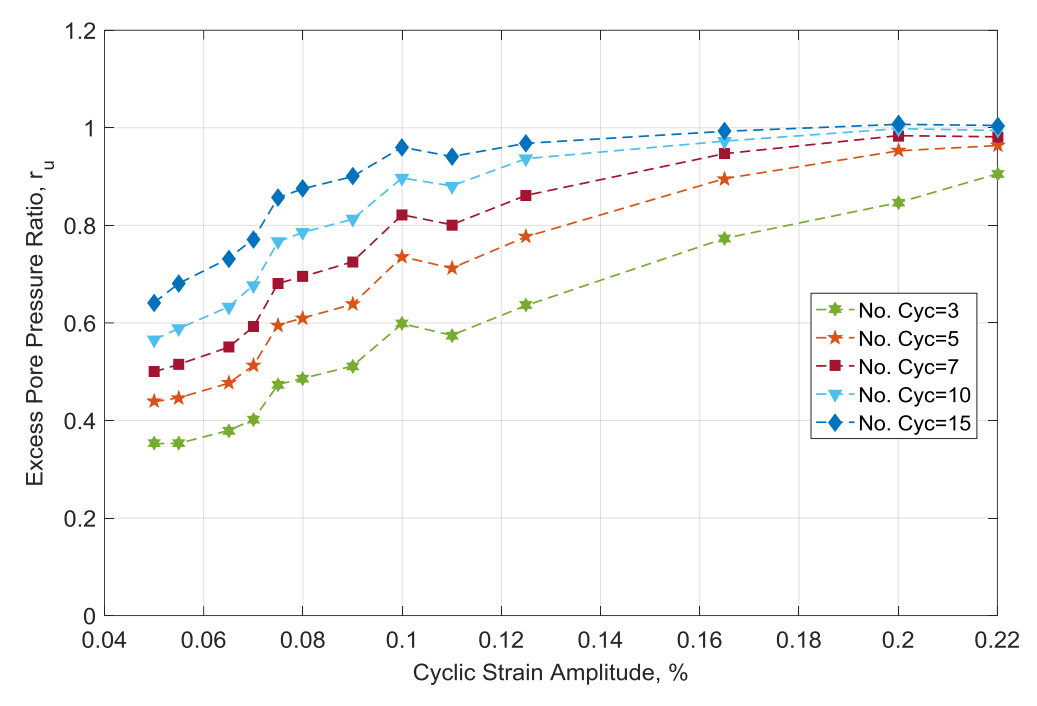


Figure 35: Excess pore pressure at different number of cycles - $e_0 = 0.608$

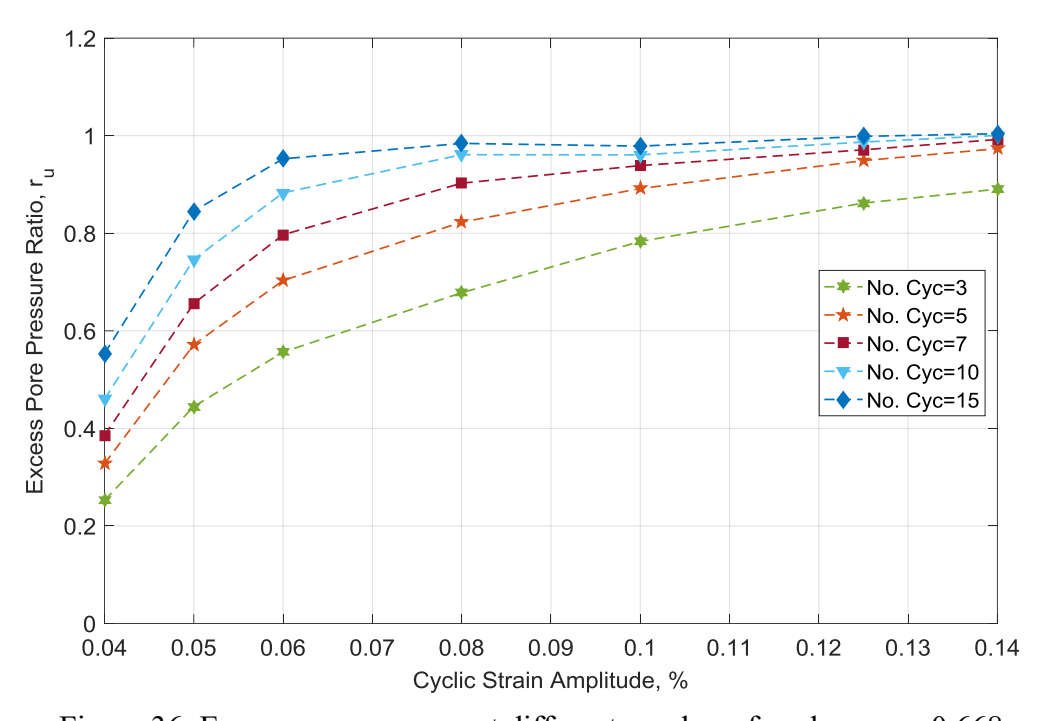


Figure 36: Excess pore pressure at different number of cycles - $e_0 = 0.668$

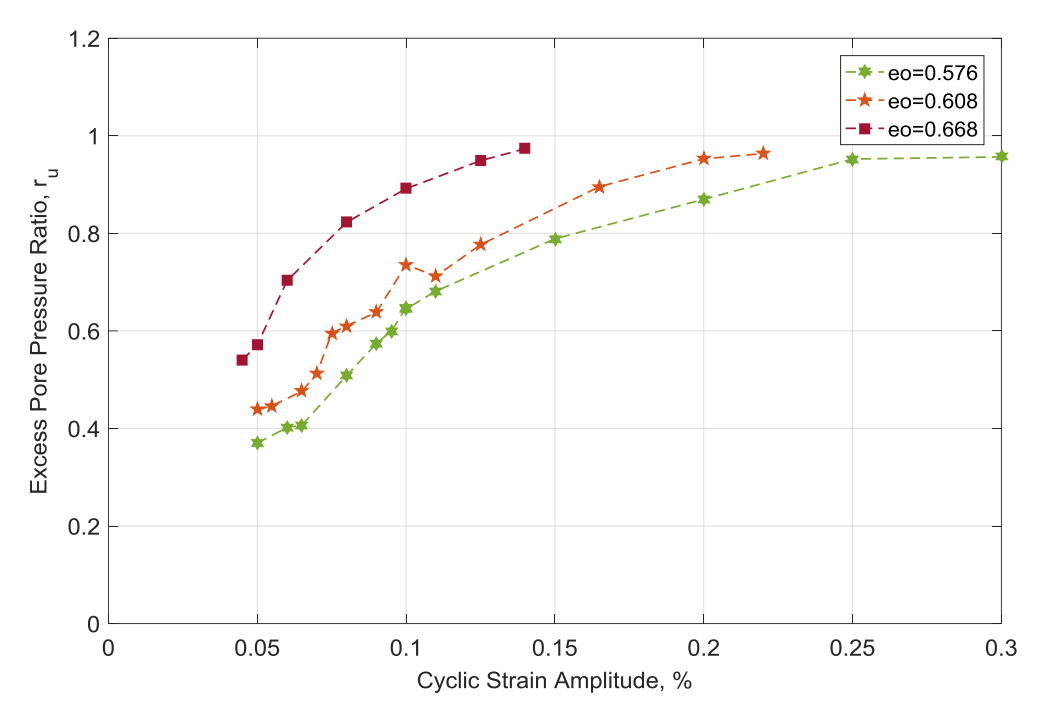


Figure 37: Excess pore pressure versus cyclic strain amplitude after 5 cycles

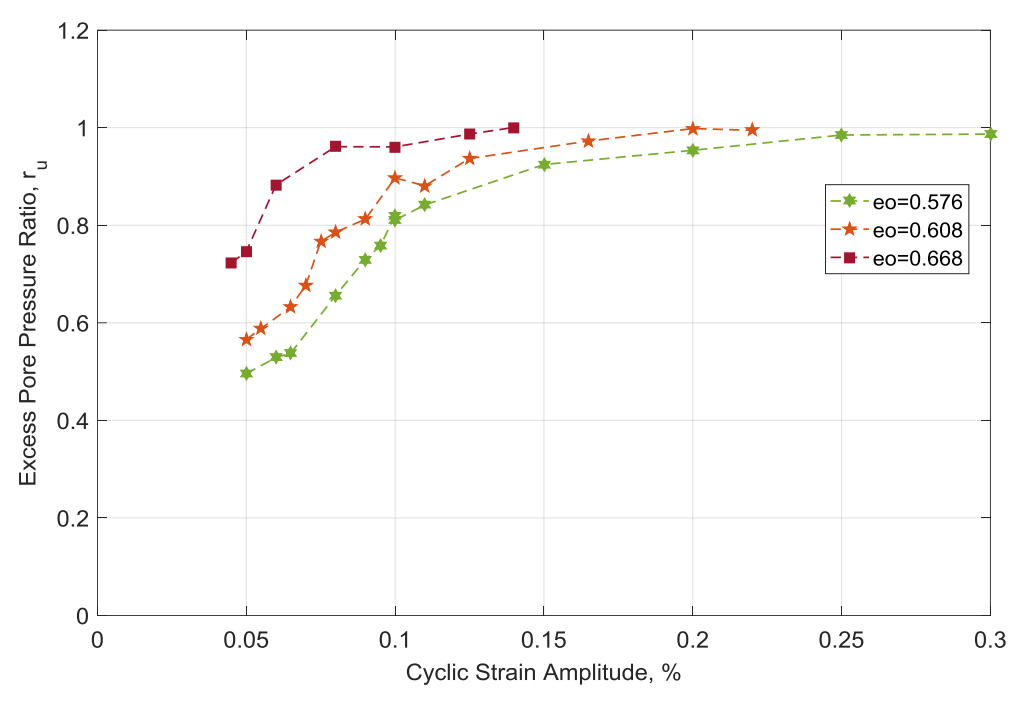


Figure 38: Excess pore pressure versus cyclic strain amplitude after 10 cycles

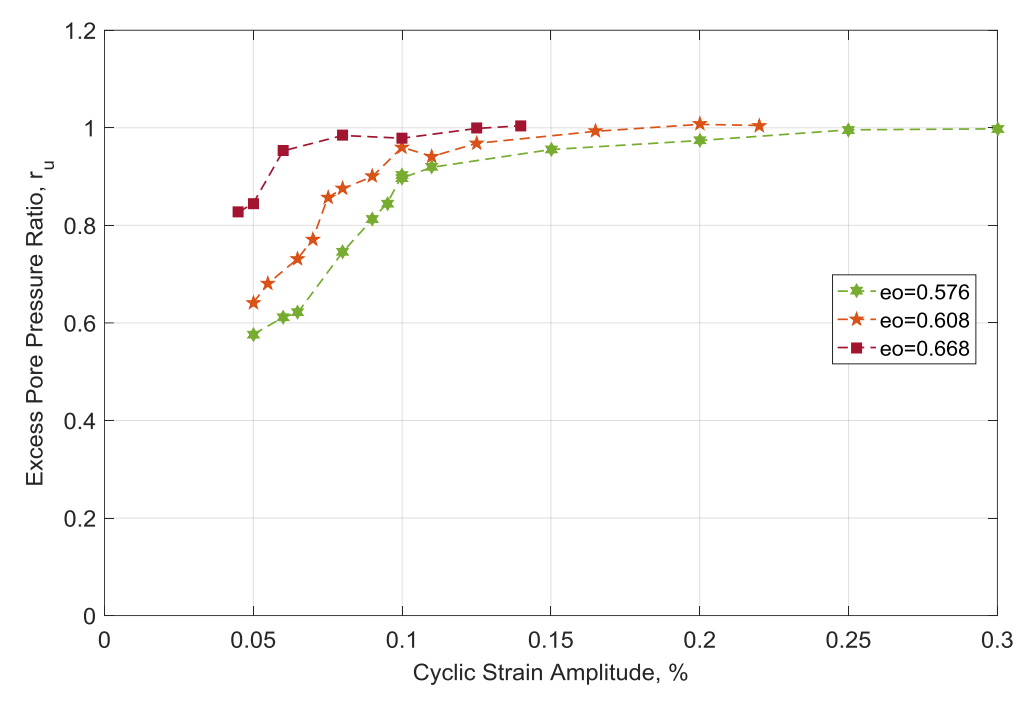


Figure 39: Excess pore pressure versus cyclic strain amplitude after 15 cycles

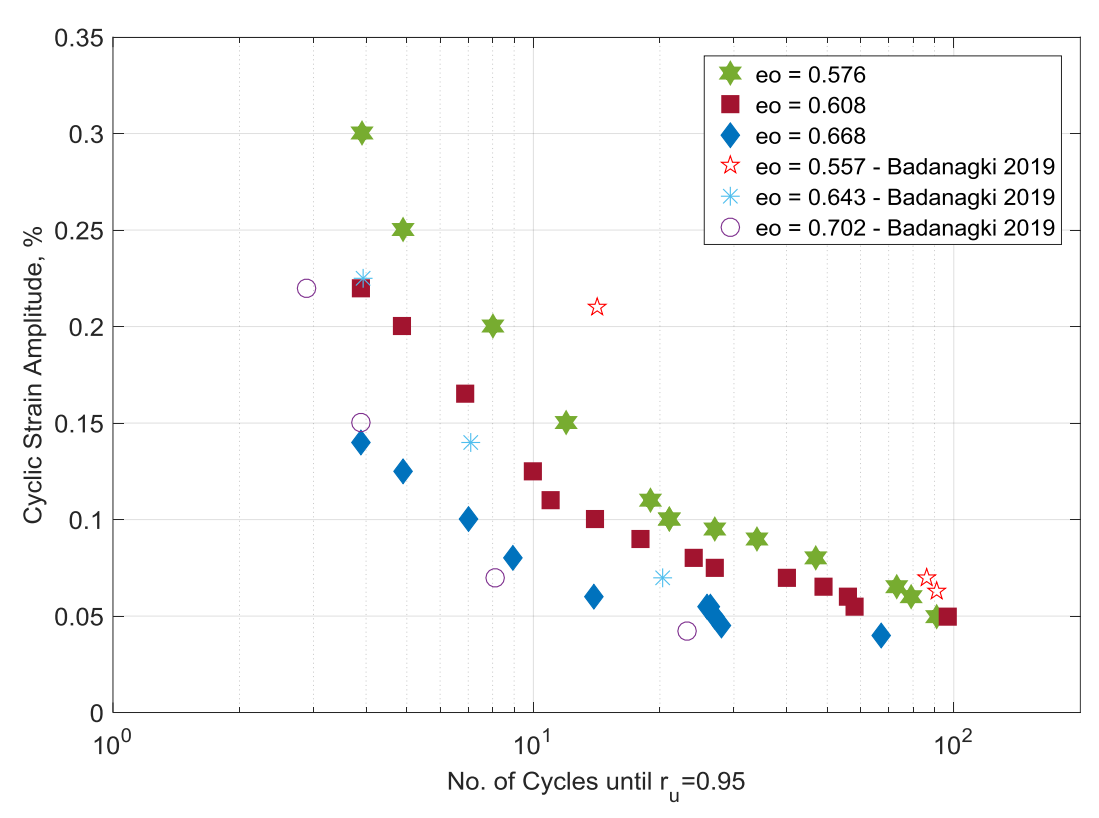


Figure 40: Liquefaction Strength Comparison with data in the literature

7. Cyclic Direct Simple Shear Tests

Two series of cyclic direct simple shear (CDSS) tests were conducted to study the effects of the overburden stress on the liquefaction strength of Ottawa F65 sand. All the tests were stress-controlled and were performed on soil specimens prepared using the CHDP method. The two sets of tests were conducted at vertical stress of 40 kPa and 100 kPa. The achieved soil density for these tests matched the density of the loosest samples tested in the cyclic triaxial experiment (reported in section 5 and 6). Tables 12 and 13 provide a summary of the key information obtained from these tests. The tables list the achieved void ratio (relative density and dry density), the applied cyclic stress ratio and the number of cycles it took to reach shear strains with double amplitudes of 1.5 %, 3.5 %, and 7.5 %.

Table 12: Summary of experiments on samples subjected to a vertical stress of 40 kPa

	$e_0=0.598 - COV=1.4\% - \sigma'_v=100 \text{ kPa}$										
Test No.	e_ac	ρ_{d}	Dr_ac	CSR	Neyc -1.5 %	Neyc -3.5 %	Neyc -7.5 %				
1	0.602	1654.5	66.03	0.16	1	6	10				
2	0.600	1656.2	66.65	0.15	4	13	17				
3	0.606	1650.3	64.51	0.14	14	26	30				
4	0.583	1673.7	72.84	0.13	54	64	69				
5	0.598	1658.3	67.39	0.11	287	295	302				
Average	0.598	1658.6	67.48								
COV (%)	1.43	0.54	4.70								

Table 13: Summary of experiments on samples subjected to a vertical stress of 100 kPa

$e_0=0.601 - COV=0.8\% - \sigma'_v=40 \text{ kPa}$								
Test No.	e_ac	ρd	Dr_ac	CSR	Neyc -1.5 %	Neyc -3.5 %	Neye -7.5 %	
1	0.597	1659.0	67.65	0.17	3	6	11	
2	0.602	1654.4	66.01	0.16	9	11	15	
3	0.596	1660.0	68.00	0.15	21	24	28	
4	0.607	1648.6	63.92	0.14	39	42	48	
5	0.604	1652.1	65.17	0.13	79	82	88	
6	0.595	1661.0	68.35	0.12	349	355	363	
Average	0.601	1654.8	66.15				_	
COV (%)	0.77	0.29	2.58					

For each test, shear wave velocity measurements using bender elements were taken after the application of vertical stress and before the shearing phase. Table 14 shows a summary of the shear wave velocity measurements and the computed shear moduli. The mean values of shear wave velocities for the specimens tested under vertical stress of 100 and 40 kPa are 41.7 MPa and 35.2 MPa, respectively. Figure 41 shows a plot of the mean and mean+/-1standard deviation.

Table 14: Shear wave velocity measurements and computed shear modulus

$\sigma'_{ m v}$	Shear Wave V	elocity, V _s	Shear Modulus, G		
(kPa)	Mean (m/sec)	COV (%)	Mean (MPa)	COV (%)	
100	159.2	1.75	41.7	3.8	
40	146	3.8	35.2	7.4	

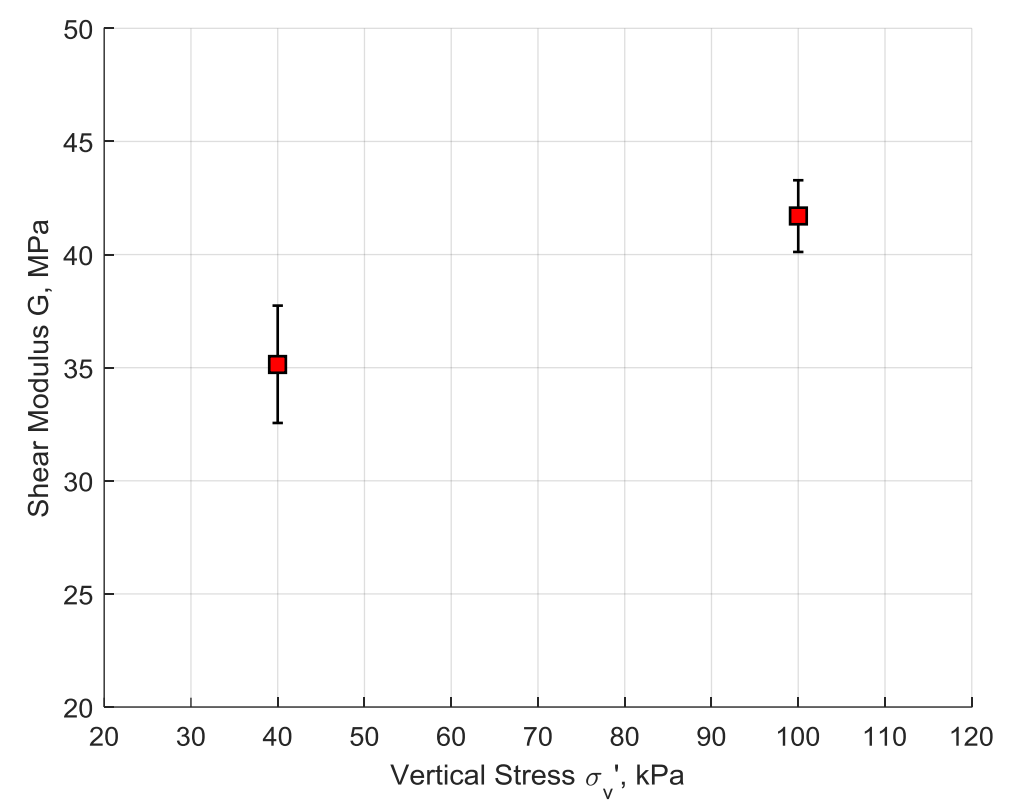


Figure 41: Shear modulus versus vertical stress

Figure 42 shows the results obtained from one of the CDSS tests where the soil specimen was subjected to vertical stress of 100 kPa and sheared with a cyclic stress ratio of 0.15. The results are plotted in terms of the stress-strain and stress path as well as the vertical stress vs. shear strain and the excess pore pressure development.

The results obtained from the CDSS experiments can also be used to develop the liquefaction strength curves. Figure 43 shows the liquefaction strength curves for the two series of tests, where the number of cycles it took to reach a double shear strain amplitude of 7.5% was considered. In addition, the number of cycles it took to reach different levels of strains (1.5%, 3.5%, and 7.5%) for each series of tests are plotted in Figures 44 and 45.

The liquefaction strength curves obtained in this study were also compared to the results of CDSS tests reported by Bastidas [17]. Figure 46 shows the liquefaction strength curves compared to the ones obtained from tests performed on samples with void ratios of 0.79 and 0.54 and

subjected to vertical stress of 50 and 100 kPa. The liquefaction curves obtained here fall in between the curves obtained by Bastidas for two different densities.

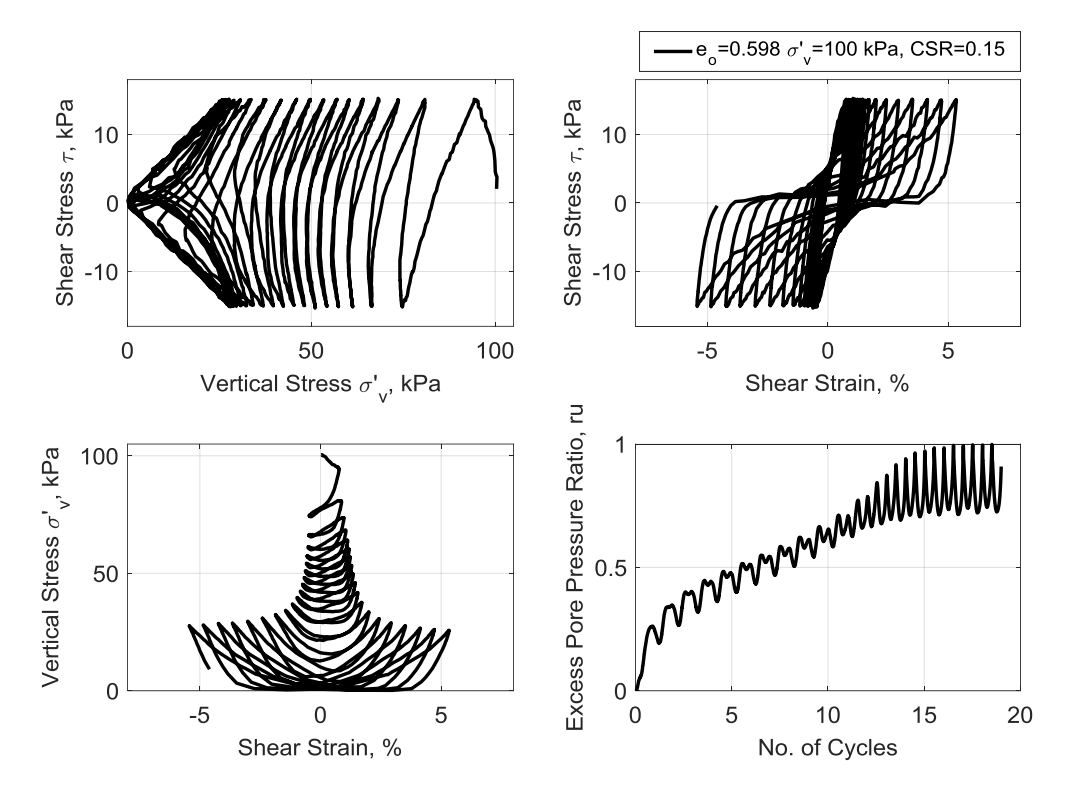


Figure 42: CDSS experiment results of Ottawa F65 sand specimen subjected to vertical stress of 100 kPa and CSR of 0.15

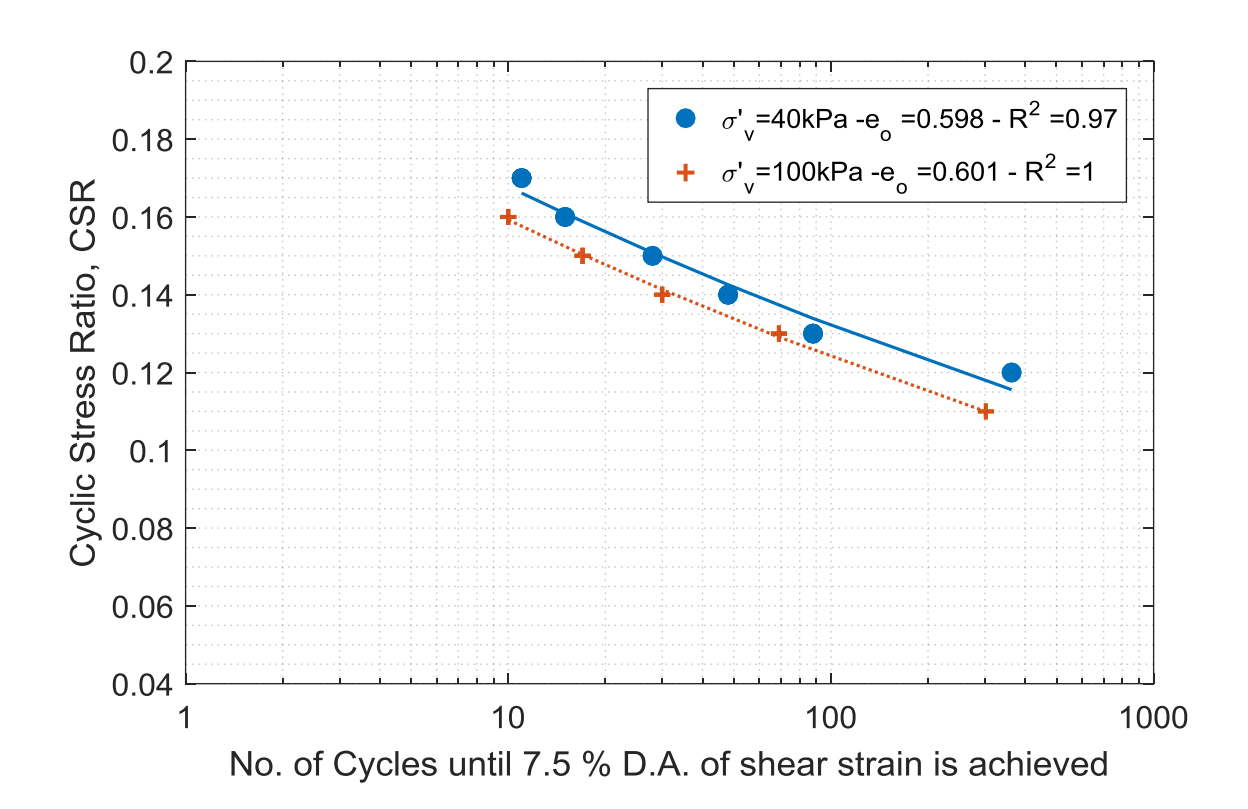


Figure 43: Liquefaction strength curves

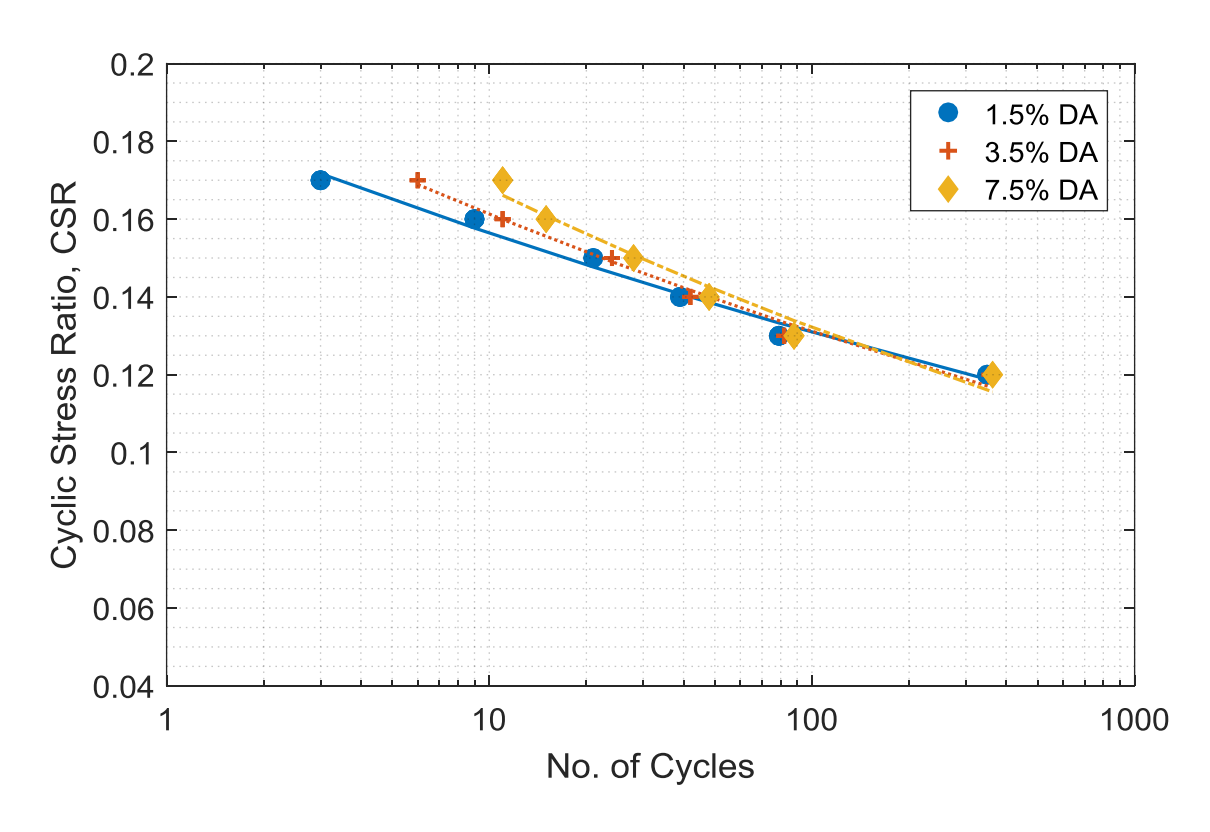


Figure 44: Number of cycles to reach different levels of shear strain – σ'_v =40 kPa

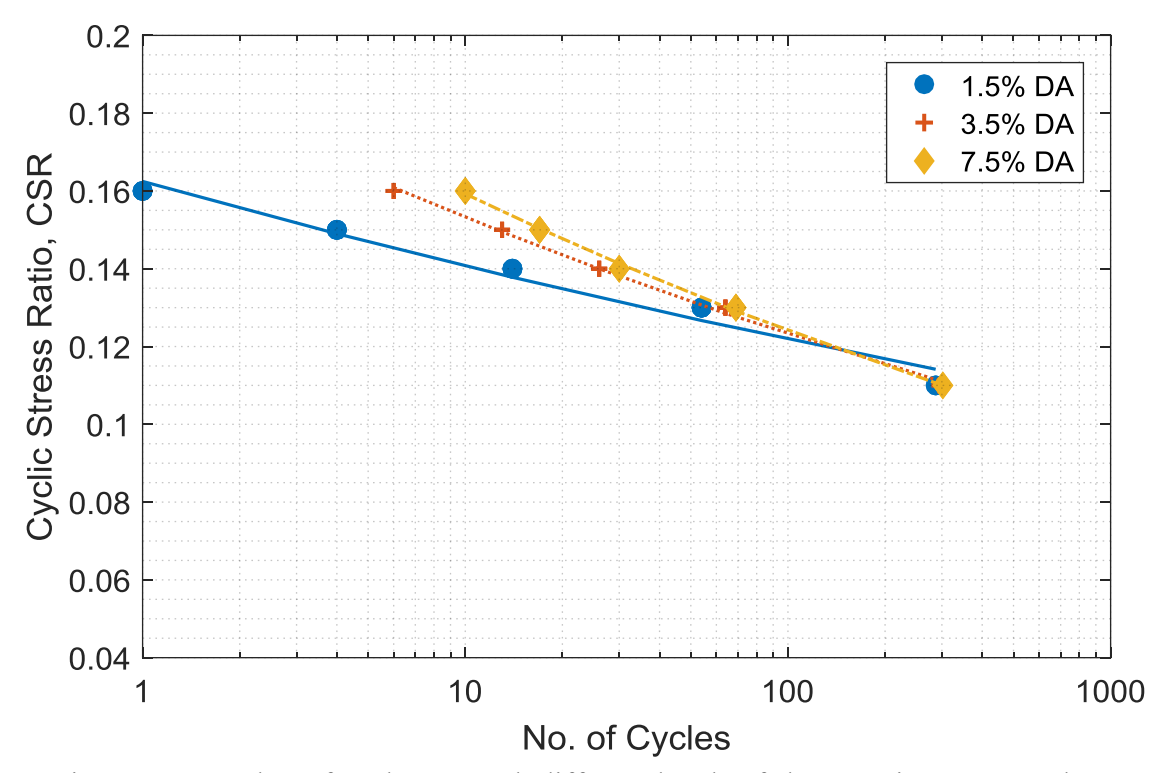


Figure 45: Number of cycles to reach different levels of shear strain – $\sigma'_v=100$ kPa

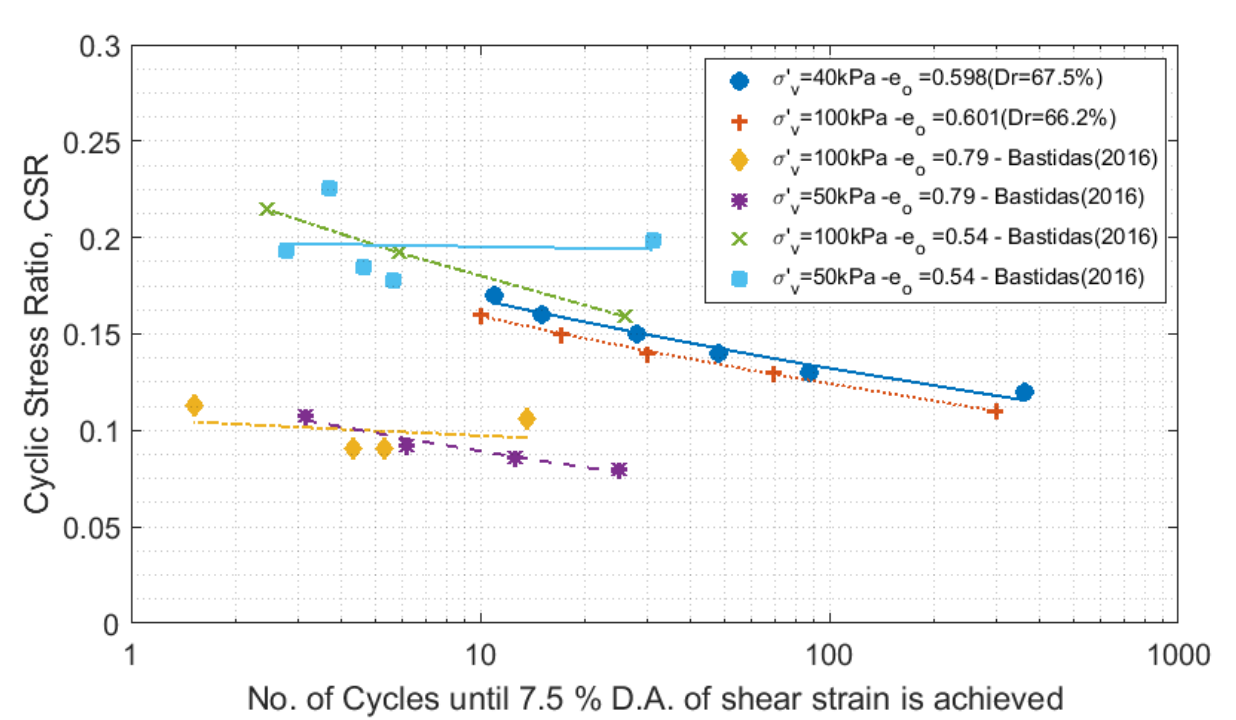


Figure 46: Liquefaction Strength Comparison with data in the literature

8. Observations

8.1. Shear Modulus Degradation

The evolution of the secant shear modulus during a cyclic test provides some useful insights on how the soil stiffness degrades with each cycle. Here, the shear modulus degradation is obtained from the experiments presented in this paper. The secant shear modulus was obtained at the first load reversal of each cycle as shown in Figure 47 for both triaxial and direct simple shear tests where G is defined as,

$$G = \frac{\tau}{\gamma} = \frac{q}{3\varepsilon_q} \tag{2}$$

In order to compare the results with each other the computed shear moduli were normalized with respect to the maximum shear modulus G_{max} which is the shear modulus of the soil under very small level of strains. Obtaining the G_{max} is not feasible from element tests as large strains develop upon loading, however, it can be obtained from the measurement of the shear wave velocity as shown in Eq. (3).

$$G_{\max} = \rho V_s^2 \tag{3}$$

As it was previously mentioned, measurements of the shear wave velocity were taken during the direct simple shear tests using bender elements (Table 14). For the triaxial tests, the G_{max} was estimated using the following relationship [26],

$$G = G_o p_{at} \frac{(2.97 - e)^2}{1 + e} \left(\frac{p}{p_{at}}\right)^{1/2}$$
 (4)

Where e is the void ratio, p is the mean effective stress and p_{at} is the atmospheric pressure. G_o is a constant shear coefficient which was assumed to be 193.3 based on the G_{max} measurements of the DSS specimens.

Figures 48 to 50 show the results obtained from the stress controlled experiments cyclic triaxial for the void ratios of 0.585, 0.542 and 0.515, respectively. Figures 51 to 53 show the results for the strain-controlled cyclic triaxial tests for void ratios of 0.668, 0.608, and 0.576, respectively. Figures 54 and 55 show the results obtained from the cyclic direct simple shear tests for vertical effective stress of 40 kPa and 100 kPa, respectively.

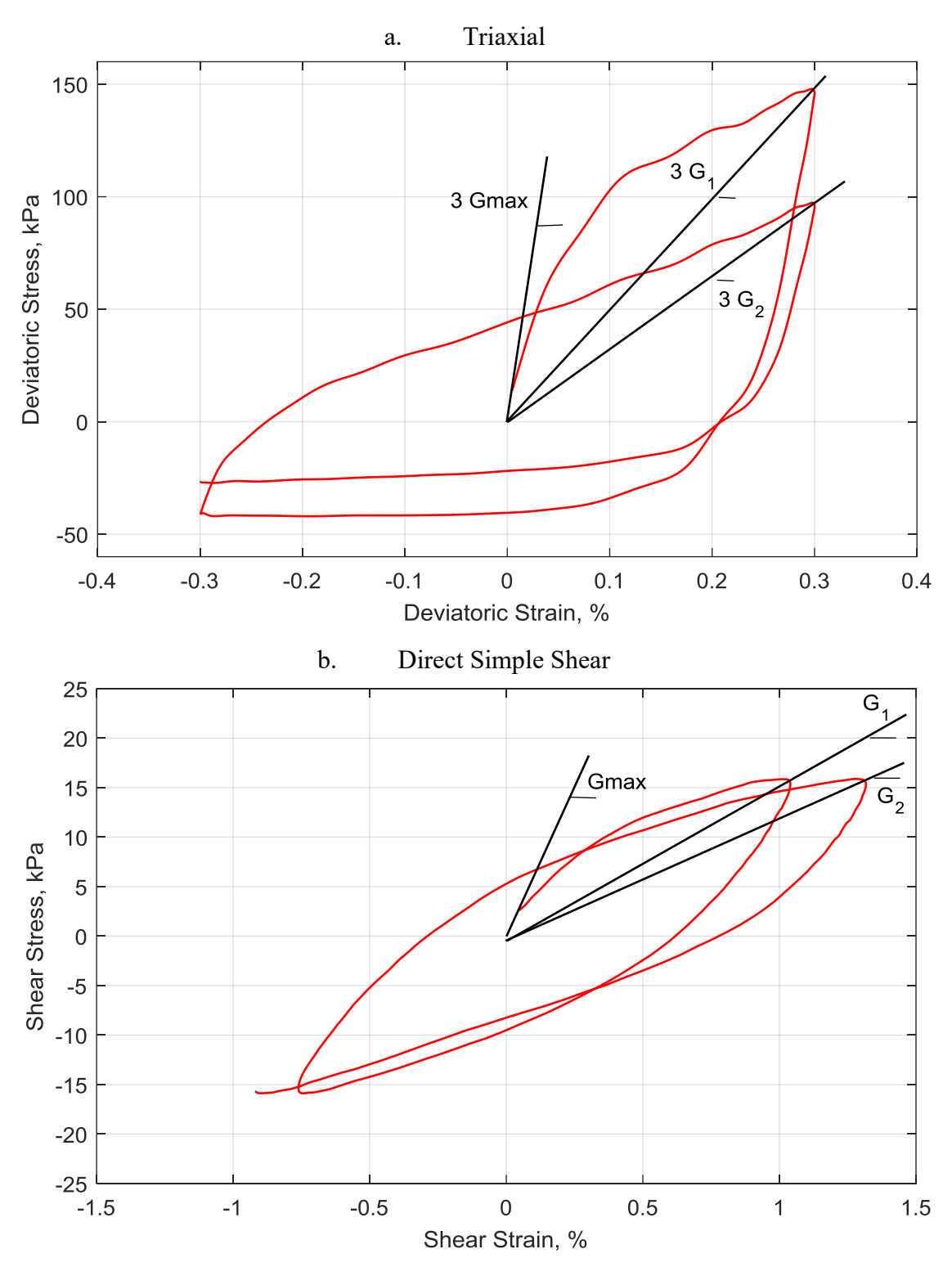


Figure 47: Secant Shear Modulus for Triaxial (a) and Direct Simple Shear (b) Tests

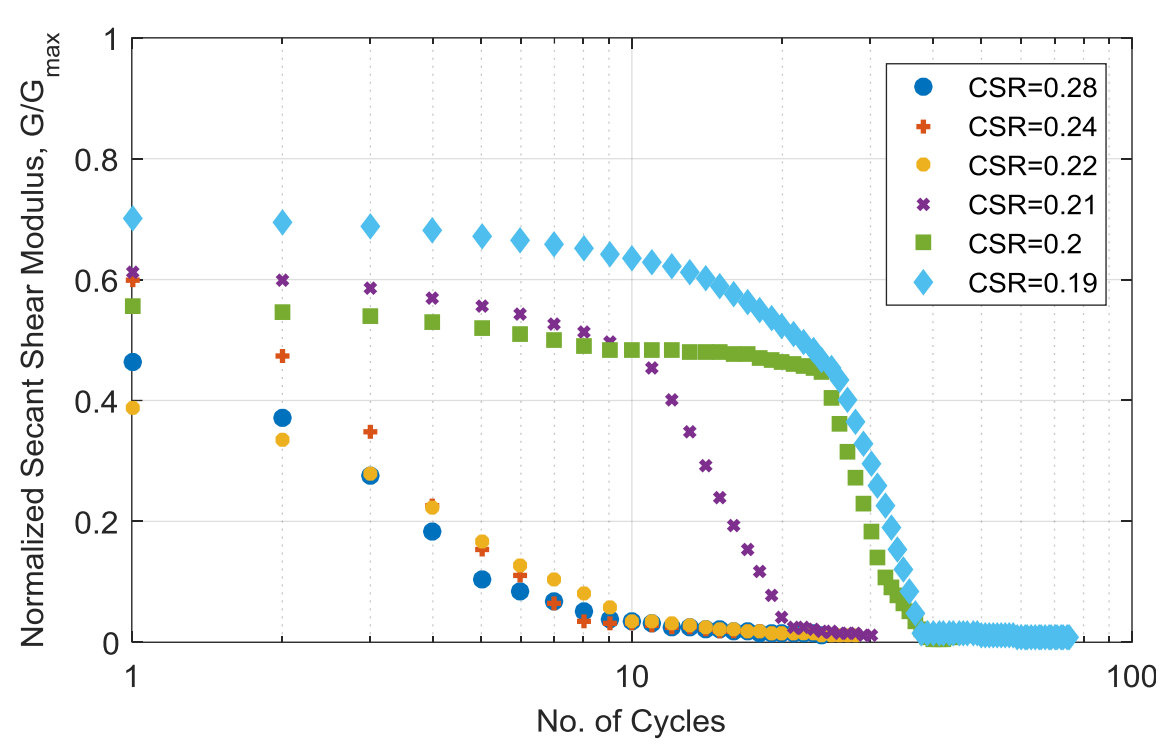


Figure 48: Secant Shear Modulus Degradation for Cyclic Triaxial Stress Controlled Tests - $e_0 = 0.585$

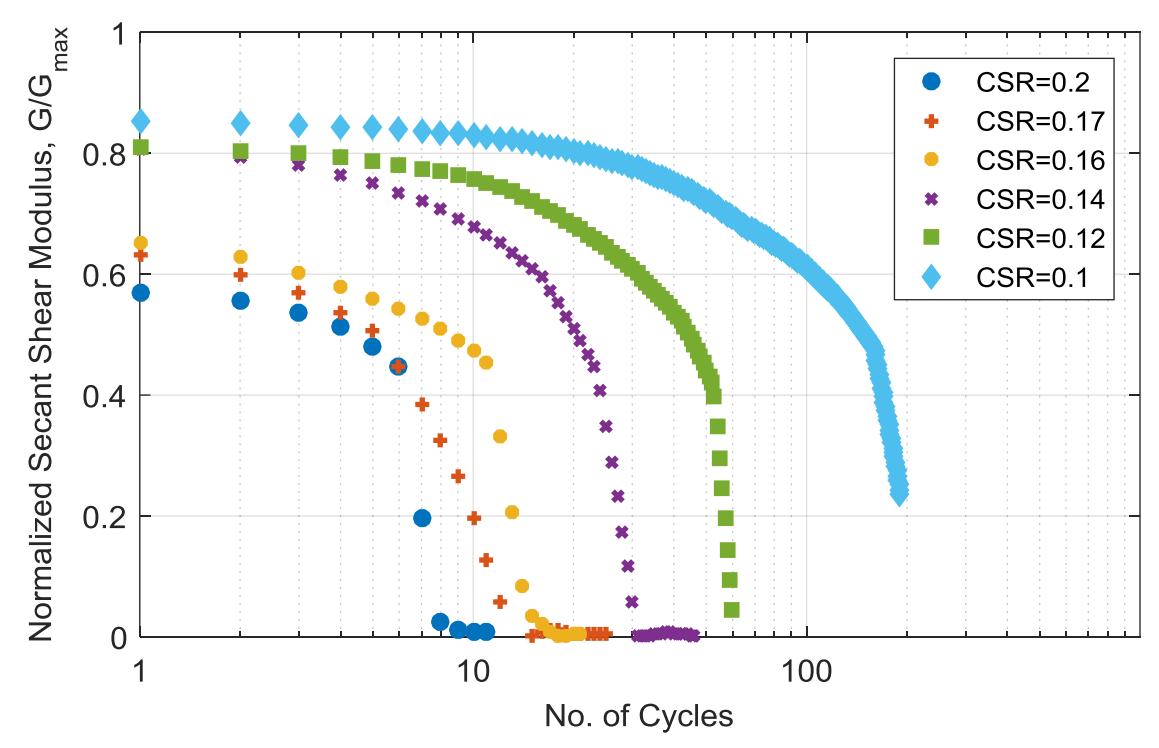


Figure 49: Secant Shear Modulus Degradation for Cyclic Triaxial Stress Controlled Tests - $e_0 = 0.542$

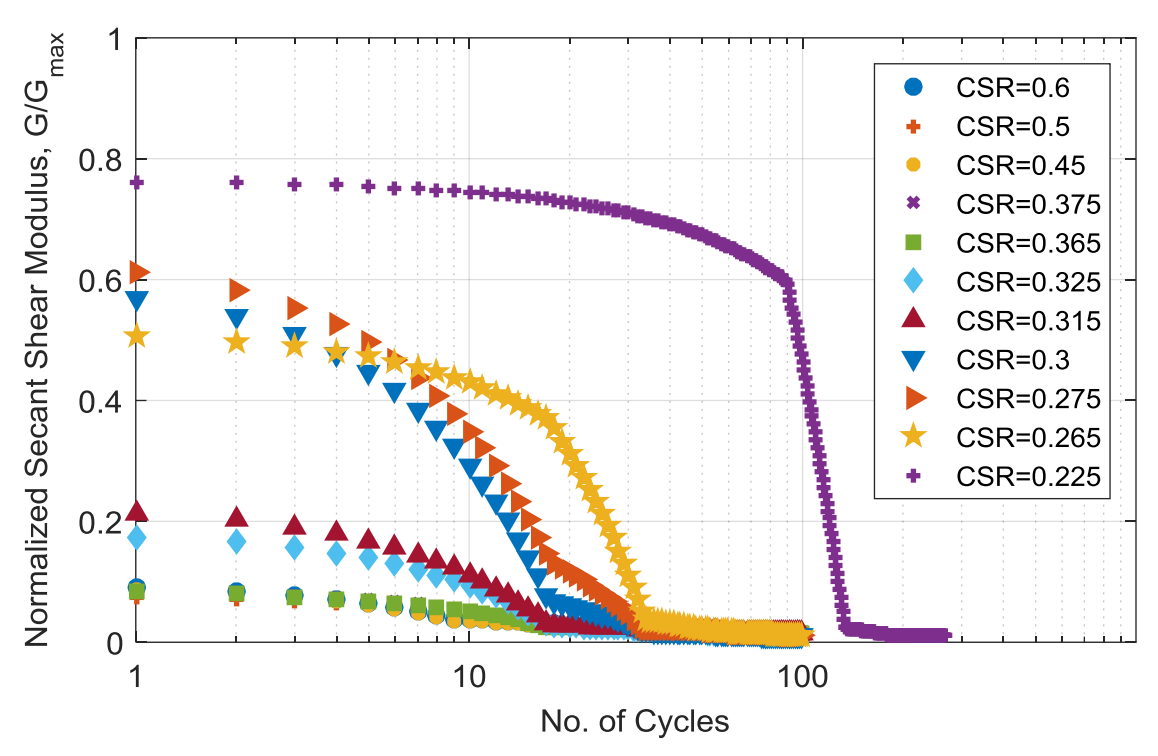


Figure 50: Secant Shear Modulus Degradation for Cyclic Triaxial Stress Controlled Tests - $e_0 = 0.515$

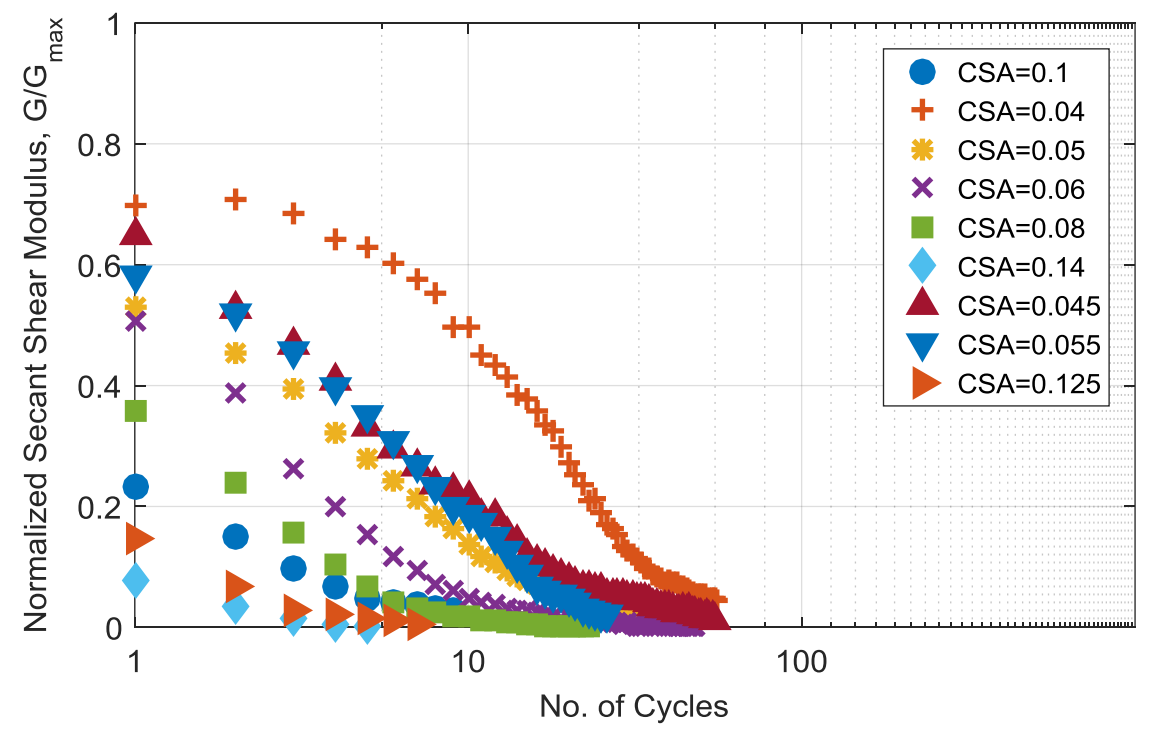


Figure 51: Secant Shear Modulus Degradation for Strain-Controlled Cyclic Triaxial Tests - $e_0 = 0.668$

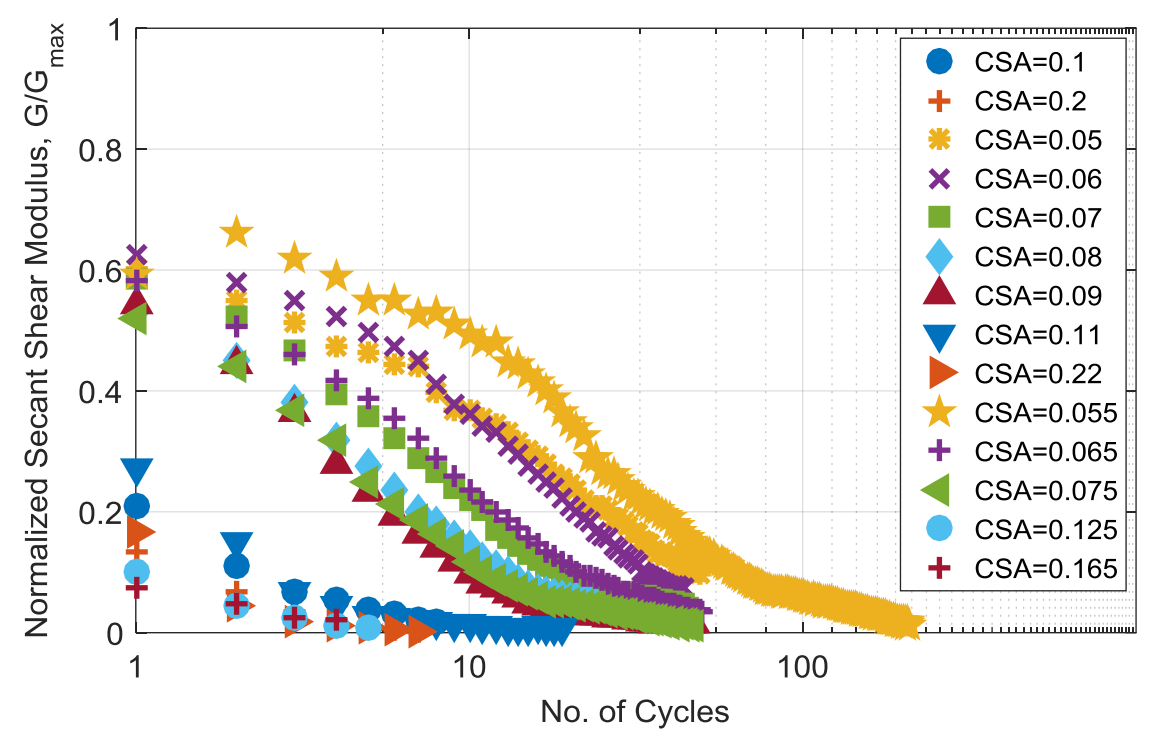


Figure 52: Secant Shear Modulus Degradation for Strain Controlled Cyclic Triaxial Tests $-e_0 = 0.608$

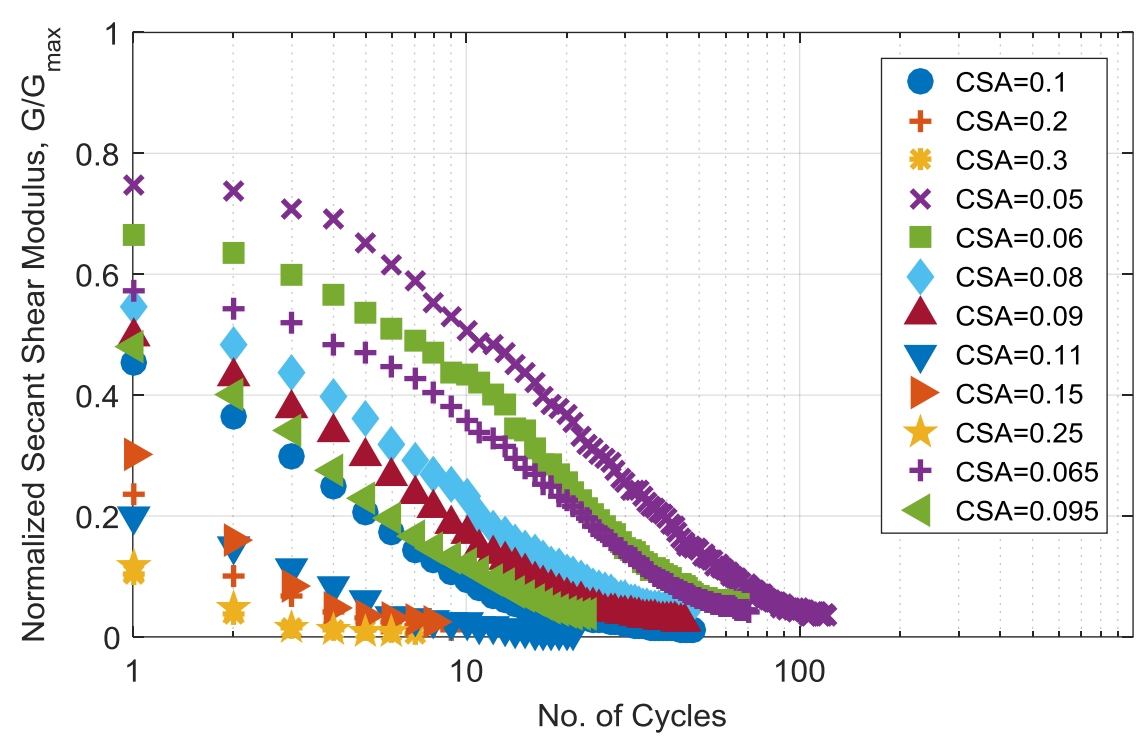


Figure 53: Secant Shear Modulus Degradation for Strain Controlled Cyclic Triaxial Tests $-e_0 = 0.576$

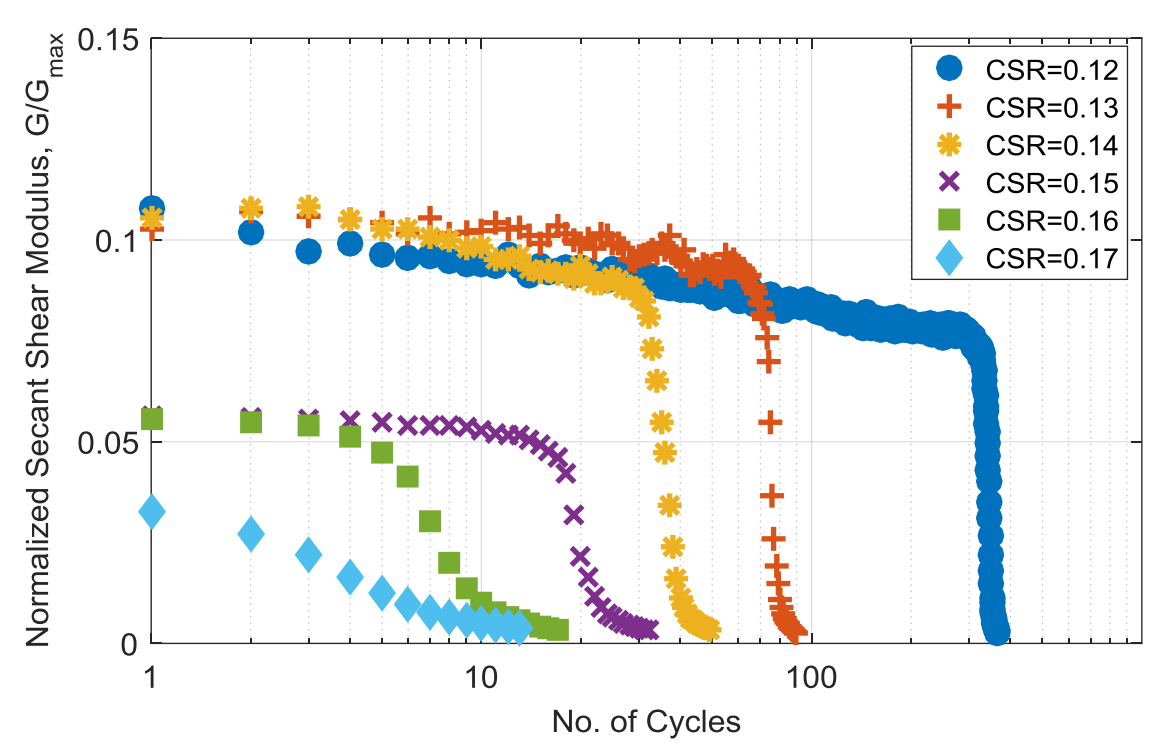


Figure 54: Secant Shear Modulus Degradation for Cyclic Direct Simple Shear Tests - σ'_v =40 kPa

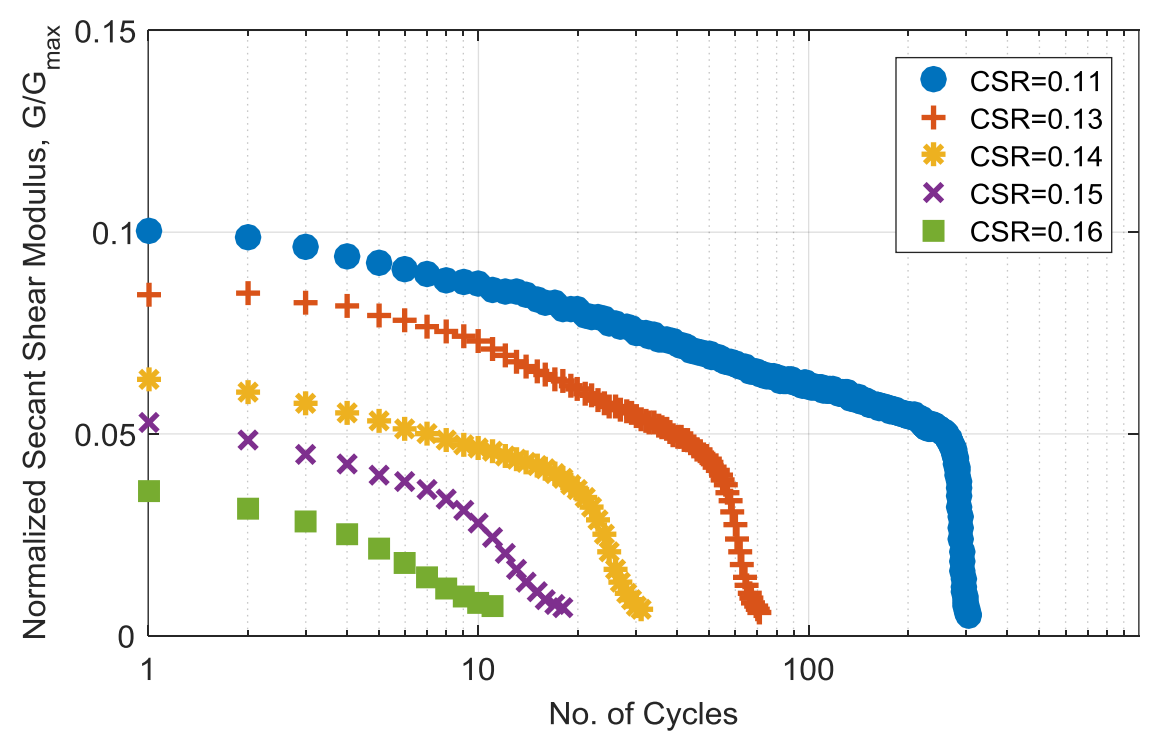


Figure 55: Secant Shear Modulus Degradation for Cyclic Direct Simple Shear Tests - $\sigma'_v = 100$ kPa

8.2. Damping

Damping curves were computed for the different tests presented in this paper. Following the method presented by Vucetic and Dobry [27], damping was computed as:

$$\lambda = \frac{1}{2\pi} \frac{\Delta E}{G\gamma_c^2} \tag{5}$$

Where ΔE is the area of the hysteresis loop for each cycle and G and γ_c are the secant shear modulus and shear strain upon the first load reversal of each cycle.

Figures 56 to 58 show the results of the damping ratio for the stress-controlled cyclic triaxial tests for void ratios 0.585, 0.542 and 0.515, respectively. Figures 59 to 60 show the damping ratio curves from the strain-controlled cyclic triaxial tests computed at the 1st, 5th and 10th cycle respectively. Figures 61 and 62 show the variation damping ratio with shear strain amplitude for the cyclic direct simple shear tests. The damping ratio peaked at a shear strain less than 0.6% for the test with initial vertical stress of 40 kPa (Figure 61) but the peak damping for the test with initial vertical stress of 100 kPa occurred at shear strains larger than 1% (Figure 62). A maximum damping ratio of about 25% was observed for both initial vertical stresses.

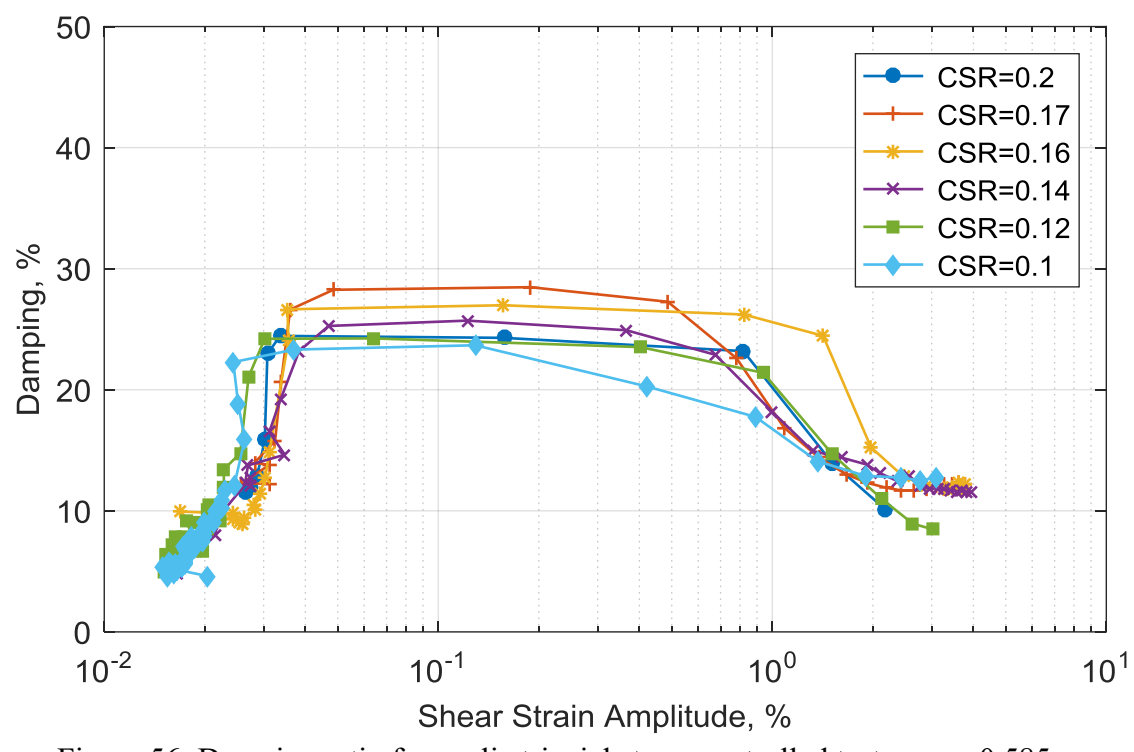


Figure 56: Damping ratio for cyclic triaxial stress controlled tests - $e_0 = 0.585$

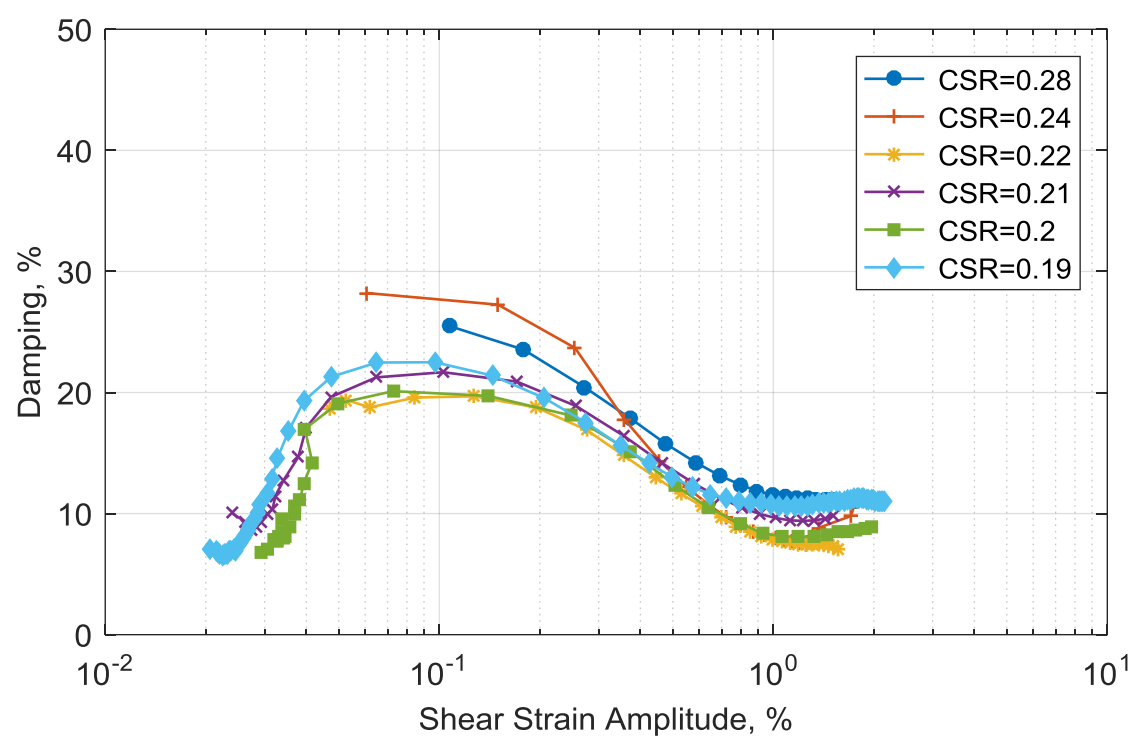


Figure 57: Damping ratio for stress-controlled cyclic triaxial tests - $e_0 = 0.542$

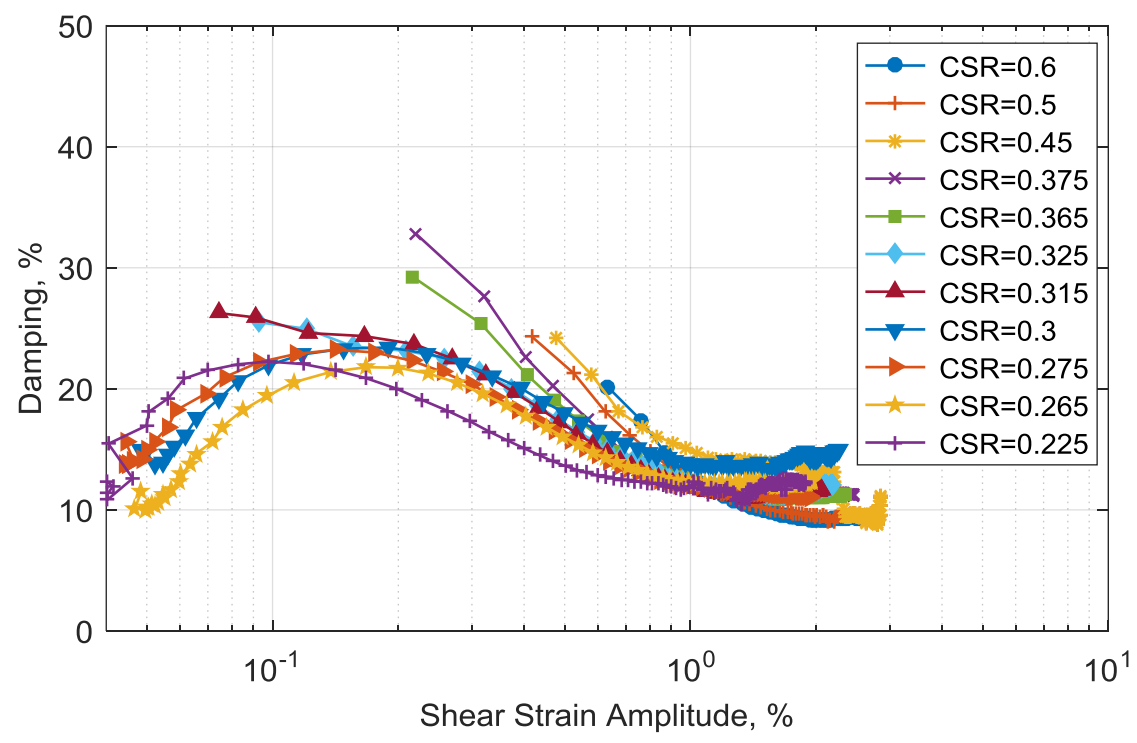


Figure 58: Damping ratio for stress-controlled cyclic triaxial tests - $e_0 = 0.515$

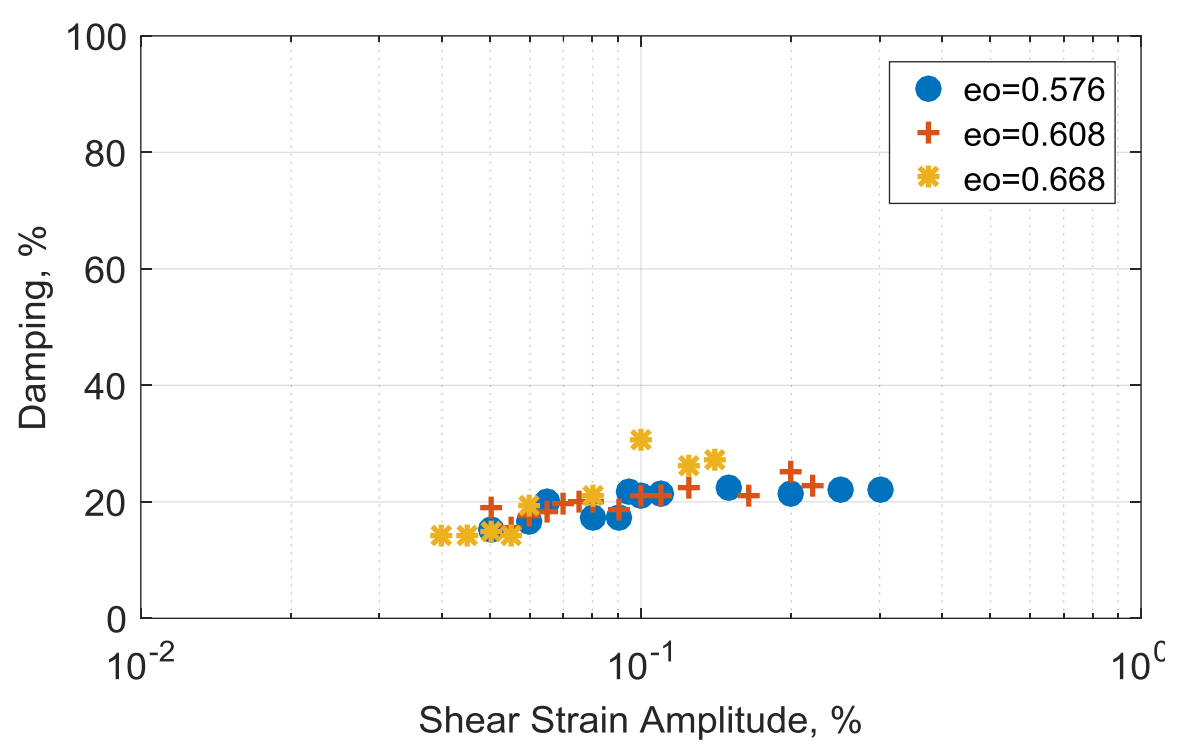


Figure 59: Damping ratio for strain-controlled cyclic triaxial test at the 1st cycle

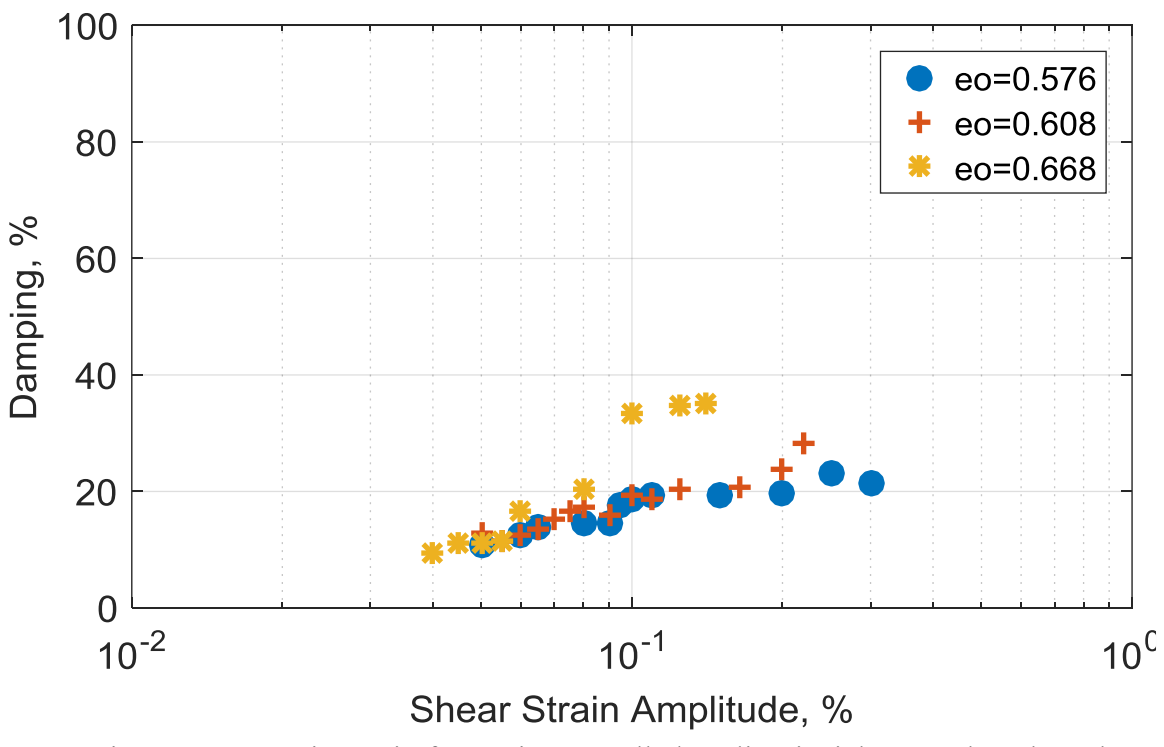


Figure 60: Damping ratio for strain-controlled cyclic triaxial test at the 5th cycle

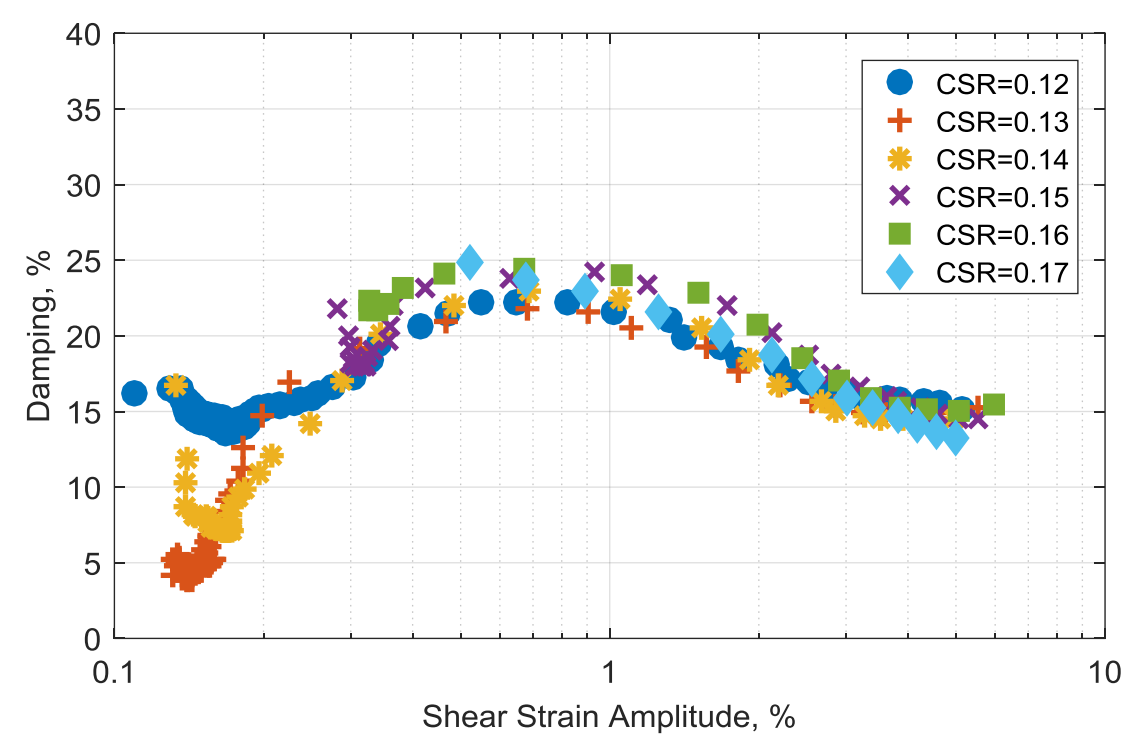


Figure 61: Damping ratio for cyclic direct simple shear tests - σ'_v =40 kPa

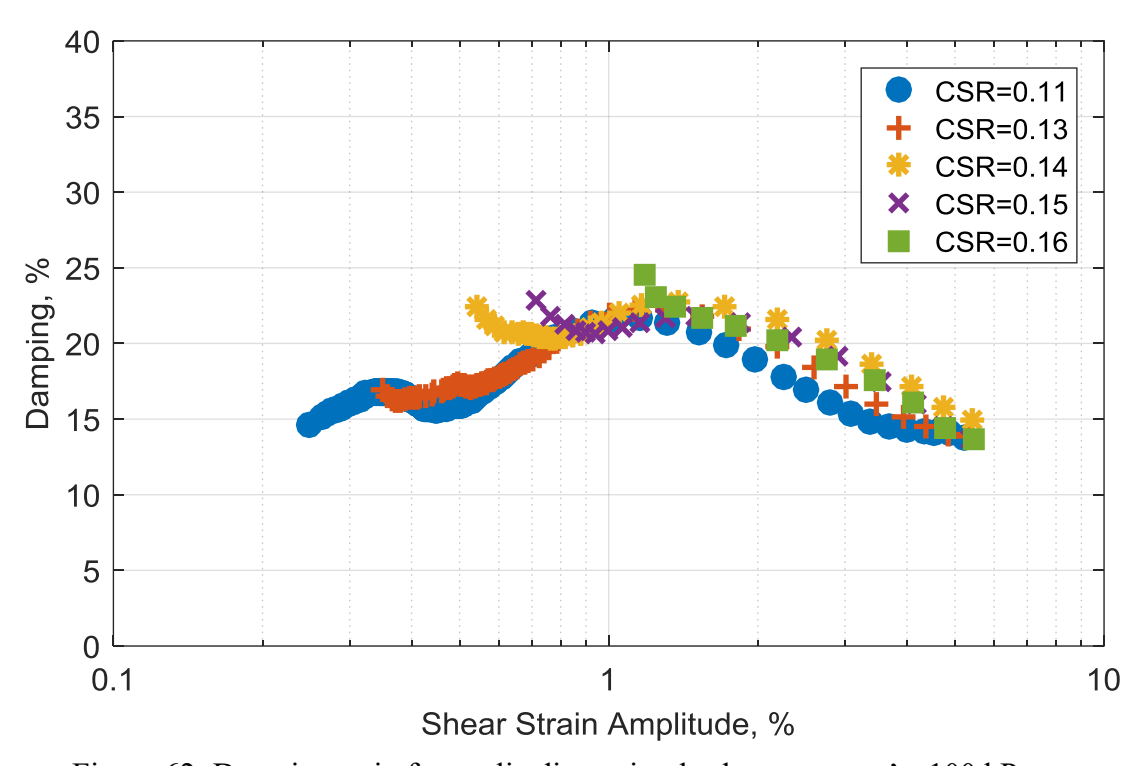


Figure 62: Damping ratio for cyclic direct simple shear tests - $\sigma'_v=100$ kPa

9. Summary and concluding remarks:

An experimental study was presented on the stress-strain response and liquefaction strength of Ottawa F65 sand. A summary of the tests conducted are as follows:

- Series of stress-controlled cyclic triaxial tests were conducted. A total of 23 experiments were performed on samples with three different densities (71.5%, 87.5%, and 97.5%).
- A total of 37 strain-controlled cyclic triaxial tests were conducted on samples with three different relative densities (40%, 63.8% and 75.6%).
- The suitability of the constant height dry pluviation sample preparation technique was evaluated by considering the repeatability of the experiments.
- A total of 11 cyclic direct simple shear tests were conducted on samples with relative density of 67.5%. The tests investigated the effects of overburden stress on the liquefaction resistance of the soil. The shear wave velocity was obtained through bender element measurements.

The data obtained from the experiments reported here were compared to the data available in the literature. There is good agreement between the tests presented here and the previously conducted tests.

The shear modulus degradation and damping curves were also computed for each test to provide a more complete picture of the soil response in cyclic loading.

The experimental work presented here along with the complete set of data available on DesignSafe are mainly intended for the use in assessment, validation and further development of constitutive models and have already been used in the calibration and numerical simulation exercises conducted during Liquefaction Experiments and Analysis Projects (LEAP) in 2015, 2017, and 2019.

10. Acknowledgment:

The planning phase of the LEAP project has been funded by the National Science Foundation grants: CMMI 1635524, CMMI 1635307 and CMMI 1635040 to the George Washington University, the University of California Davis, and Rensselaer Polytechnic Institute, respectively. This support is gratefully acknowledged.

11. References:

- [1] Seed B, Lee K. Liquefaction of Saturated Sands During Cyclic Loading. J Soil Mech Found Div Proc Am Soiciety Civ Eng 1966;92:105–34.
- [2] Castro G. Liquefaction of Sands. 1969.
- [3] Jefferies M, Been K. Soil Liquefaction: A Critical State Approach. Second Edi. London:

- CRC Press; 2016.
- [4] Castro G, Poulos SJ. Factors Affecting Liquefaction and Cyclic Mobility. J Geotech Eng Div 1977;103.
- [5] Wichtmann T, Triantafyllidis T. Behaviour of Granular Soils Under Environmentally Induced Cyclic Loads. Mech. Behav. Soils Under Environ. Induc. Cycl. Loads, vol. 534, Udine: CISM; 2012, p. 1–136. https://doi.org/10.1007/978-3-7091-1068-3.
- [6] Ishihara K. Soil Behaviour in Earthquake Geotechnics. 1996.
- [7] Vaid YP, Finn WDL. Static Shear and Liquefaction Potential. J Geotech Eng Div 1979;105:1233–46.
- [8] Rollins KM, Seed HB. Influence of buildings on potential liquefaction damage. J Geotech Eng 1990;116:165–85. https://doi.org/10.1061/(ASCE)0733-9410(1990)116:2(165).
- [9] Mulilis JP, Chan CK, Seed HB. The effects of method of sample preparation on the cyclic stress-strain behavior of sands. 1975.
- [10] Manzari MT, ElGhoraiby M, Kutter BL, Zeghal M, Abdoun T, Arduino P, et al. Liquefaction experiment and analysis projects (LEAP): Summary of observations from the planning phase. Soil Dyn Earthq Eng 2017. https://doi.org/10.1016/j.soildyn.2017.05.015.
- [11] Manzari MT, Ghoraiby M El, Zeghal M, Kutter BL, Arduino P, Barrero AR, et al. LEAP-2017 Simulation Exercise: Calibration of Constitutive Models and Simulation of the Element Tests. Cham: Springer International Publishing; 2020. https://doi.org/10.1007/978-3-030-22818-7.
- [12] Manzari MT, El Ghoraiby M, Zeghal M, Kutter BL, Arduino P, Barrero AR, et al. LEAP-2017: Comparison of the Type-B Numerical Simulations with Centrifuge Test Results. Model Tests Numer. Simulations Liq. Lateral Spreading, Cham: Springer International Publishing; 2020, p. 187–218. https://doi.org/10.1007/978-3-030-22818-7_10.
- [13] Kutter BL, Carey TJ, Hashimoto T, Zeghal M, Abdoun T, Kokkali P, et al. LEAP-GWU-2015 experiment specifications, results, and comparisons. Soil Dyn Earthq Eng 2017;113:616–28. https://doi.org/10.1016/j.soildyn.2017.05.018.
- [14] Kutter BL, Carey TJ, Stone N, Zheng BL, Gavras A, Manzari MT, et al. LEAP-UCD-2017 Comparison of Centrifuge Test Results. Cham: Springer International Publishing; 2020. https://doi.org/10.1007/978-3-030-22818-7.
- [15] Ueda K. LEAP-Asia-2019. Priv Commun 2019.
- [16] Vasko A. An Investigation into the Behavior of Ottawa Sand through Monotonic and Cyclic Shear Tests. George Washington University, 2015.
- [17] Bastidas AMB. Ottawa F-65 Sand Characterization. University of California, Davis, 2016.
- [18] Vasko A, ElGhoraiby MA, Manzari MT. LEAP-GWU-2015 Laboratory Tests. Dataset 2018. https://doi.org/10.17603/DS2TH7Q.

- [19] Ueda K, Vargas R, Uemura K. Cyclic Torsional Shear Tests 2018. https://doi.org/10.17603/DS28D8G.
- [20] Carey TJ, Stone N, Kutter BL. Grain Size Analysis and Maximum and Minimum Dry Density of Ottawa F-65 Sand for LEAP-UCD-2017 2017.
- [21] ElGhoraiby M. Modeling of Liquefaction-Induced Lateral Spreading. George Washington University, 2019.
- [22] ElGhoraiby M, Park H, Manzari MT. Physical and Mechanical Properties of Ottawa F65 Sand. In: Kutter B, Manzari M, Zeghal M, editors. Model Tests Numer. Simulations Liq. Lateral Spreading, Springer In press; 2019, p. 41–62.
- [23] ElGhoraiby MA, Park H, Manzari MT. LEAP-2017 GWU Laboratory Tests 2018. https://doi.org/10.17603/DS2210X.
- [24] Badanagki MA. Centrifuge Modeling of Dense Granular Columns in Layered Liquefiable Soils with Varying Stratigraphy and Overlying Structures. University of Colorado, Boulder, 2019.
- [25] Ramirez J, Badanagki M, Rahimi Abkenar M, ElGhoraiby MA, Manzari MT, Dashti S, et al. Seismic Performance of a Layered Liquefiable Site: Validation of Numerical Simulations Using Centrifuge Modeling. Geotech Front 2017 2017:332–41. https://doi.org/10.1061/9780784480489.033.
- [26] Richart FE, Hall JR, Woods RD. Vibrations of Soils and Foundations. Englewood Cliffs, N.J.: Prentice Hall; 1970.
- [27] Vucetic M, Dobry R. Effect of Soil Plasticity on Cyclic Response. J Geotech Eng 1991;117.